VALIDATION OF OUTGOING LONGWAVE RADIATION IN THE GLAS GENERAL CIRCULATION MODEL

by

Gerald R. Borger

Thesis submitted to the Faculty of the Graduate School
of the University of Maryland in partial fulfillment
of the requirements for the degree of
Master of Science
1985

UNCLASS

SECURITY CLASSIFICATION OF THIS PAGE (When Data Entered)

1

REPORT DOCUMENTATION PAGE		READ INSTRUCTIONS BEFORE COMPLETING FORM
1. REPORT NUMBER AFIT/CI/NR 85-55T	2. GOVT ACCESSION NO.	3. RECIPIENT'S CATALOG NUMBER
4. TITLE (and Subtitle) Validation of Outgoing Longwave Radiation in the GLAS General Circulation Model		5. TYPE OF REPORT & PERIOD COVERED THESIS/DISSERTATION 6. PERFORMING ORG. REPORT NUMBER
7. AUTHOR(s) Gerald R. Borger		8. CONTRACT OR GRANT NUMBER(s)
9. PERFORMING ORGANIZATION NAME AND ADDRESS AFIT STUDENT AT: University of Maryland		10. PROGRAM ELEMENT, PROJECT, TASK AREA & WORK UNIT NUMBERS
11. CONTROLLING OFFICE NAME AND ADDRESS AFIT/NR WPAFB OH 45433		12. REPORT DATE 1985 13. NUMBER OF PAGES 65
14. MONITORING AGENCY NAME & ADDRESS(if different from Controlling Office)		15. SECURITY CLASS. (of this report) UNCLASS 15a. DECLASSIFICATION/DOWNGRADING SCHEDULE

16. DISTRIBUTION STATEMENT (of this Report)

APPROVED FOR PUBLIC RELEASE; DISTRIBUTION UNLIMITED

DTIC ELECTE AUG 16 1985 S D

17. DISTRIBUTION STATEMENT (of the abstract entered in Block 20, if different from Report)

B

18. SUPPLEMENTARY NOTES

APPROVED FOR PUBLIC RELEASE: IAW AFR 190-1

5 AUG 1985

LYNN E. WOLAVER
Dean for Research and
Professional Development
AFIT, Wright-Patterson AFB OH

19. KEY WORDS (Continue on reverse side if necessary and identify by block number)

20. ABSTRACT (Continue on reverse side if necessary and identify by block number)

ATTACHED

AD-A158 006

DTIC FILE COPY

DD FORM 1 JAN 73 1473 EDITION OF 1 NOV 65 IS OBSOLETE

UNCLASS

SECURITY CLASSIFICATION OF THIS PAGE (When Data Entered)

85 8 13 096

ABSTRACT

Title of Thesis: "Validation of Outgoing Longwave Radiation in the GLAS General Circulation Model", 65 pg.

Gerald R. Borger, Capt, USAF
Master of Science, 1985
University of Maryland

Thesis directed by: Anandu D. Vernekar, Professor
Department of Meteorology

Outgoing longwave radiation (OLR) simulated by the GLAS general circulation model is validated with that derived from measurements made by polar orbiting satellites. The mean observed and simulated OLR fields are compared for spatial and seasonal variations by expanding them into spherical surface harmonics. The student's 't' test is used to determine the significance of differences between the simulated and observed fields.

The global mean and standard deviation of the simulated geographical fields are respectively about 20 Wm^{-2} smaller and 10 Wm^{-2} larger than the corresponding values of the observed field. The major fraction of the variability in the simulated field is due to a sharp meridional gradient in the field. The seasonal variation of the global mean and standard deviation of the simulated fields are in good agreement with observations. Correlation coefficients between the observed and simulated fields as a function of spatial scales show that the phase relationship for large spatial scales is

very good for January and July months but fair for April and October. In the tropics, the differences between simulated and observed OLR means are not significantly different from zero, except over deep convection regions (Asiatic monsoon, Amazon, Central Africa) where the model convective clouds do not interact with radiation. The differences in the middle and high latitudes are highly significant, more so in the southern hemisphere than in the northern hemisphere.

AFIT RESEARCH ASSESSMENT

The purpose of this questionnaire is to ascertain the value and/or contribution of research accomplished by students or faculty of the Air Force Institute of Technology (AU). It would be greatly appreciated if you would complete the following questionnaire and return it to:

AFIT/NR
Wright-Patterson AFB OH 45433

RESEARCH TITLE: Validation of Outgoing Longwave Radiation in the GLAS General Circulation Model

AUTHOR: Gerald R. Borger

RESEARCH ASSESSMENT QUESTIONS:

1. Did this research contribute to a current Air Force project?

( ) a. YES ( ) b. NO

2. Do you believe this research topic is significant enough that it would have been researched (or contracted) by your organization or another agency if AFIT had not?

( ) a. YES ( ) b. NO

3. The benefits of AFIT research can often be expressed by the equivalent value that your agency achieved/received by virtue of AFIT performing the research. Can you estimate what this research would have cost if it had been accomplished under contract or if it had been done in-house in terms of manpower and/or dollars?

( ) a. MAN-YEARS _____ ( ) b. $_____

4. Often it is not possible to attach equivalent dollar values to research, although the results of the research may, in fact, be important. Whether or not you were able to establish an equivalent value for this research (3. above), what is your estimate of its significance?

( ) a. HIGHLY SIGNIFICANT ( ) b. SIGNIFICANT ( ) c. SLIGHTLY SIGNIFICANT ( ) d. OF NO SIGNIFICANCE

5. AFIT welcomes any further comments you may have on the above questions, or any additional details concerning the current application, future potential, or other value of this research. Please use the bottom part of this questionnaire for your statement(s).

NAME GRADE POSITION

ORGANIZATION LOCATION

STATEMENT(s):

FOLD DOWN ON OUTSIDE - SEAL WITH TAPE

AFIT/NR
WRIGHT-PATTERSON AFB OH 45433

OFFICIAL BUSINESS
PENALTY FOR PRIVATE USE, $300

NO POSTAGE
NECESSARY
IF MAILED
IN THE
UNITED STATES

BUSINESS REPLY MAIL
FIRST CLASS PERMIT NO. 73236 WASHINGTON D.C.

POSTAGE WILL BE PAID BY ADDRESSEE

AFIT/ DAA
Wright-Patterson AFB OH 45433

FOLD IN

APPROVAL SHEET

Title of Thesis: Validation of Outgoing Longwave Radiation in the GLAS General Circulation Model

Name of Candidate: Gerald R. Borger
Master of Science, 1985

Thesis and Abstract Approved: Anandu D. Vernekar
Anandu D. Vernekar
Professor
Department of Meteorology

Date Approved: April 25, 1985

CURRICULUM VITAE

Name: Gerald Ray Borger

PII Redacted [redacted]

Degree and date to be conferred: M.S., 1985.

[redacted]

[redacted]

Secondary education: State College Area High School
State College, PA May, 1971.

Collegiate institutions attended	Dates	Degree	Date of degree
University of Maryland College Park, MD	8/83- 5/85	M.S.	5/85
Pennsylvania State University University Park, PA	5/77- 5/79	B.S.	5/79
Pennsylvania State University University Park, PA	6/71-10/72		

Major: Meteorology

Positions Held: Weather Liaison Officer Hq Air Force Global Weather Central, Offutt, AFB, NE.

Weather Liaison Officer, 5th Weather Wing, Langley AFB, VA.

ACKNOWLEDGMENT

A great many people have generously offered their assistance in helping me complete this thesis. While I am grateful to all, I wish to specifically thank Mr Bert Katz for his instruction on spherical harmonics, and Mr Mike Fennessey for his help in locating technical information on the GLAS model. Most of all I'd like to express my gratitude to my advisor, Dr Anandu Vernekar, for his patience in our many discussions, for his instruction and review, and for making a potentially tedious project both interesting and satisfying.

TABLE OF CONTENTS

1. Introduction	1
2. Satellite Data	4
3. The GLAS Model	8
4. Spherical Harmonics	15
5. Analysis and Results	20
6. Conclusions	48
Appendix I: Calculations	51
Appendix II: Amplitudes	54
Appendix III: Variances	58
Bibliography	62

LIST OF TABLES

Table 1: Equator Crossing Times 5

Table 2: January and April Correlation Coefficients 36

Table 3: July and October Correlation Coefficients 37

LIST OF FIGURES

1a. Simulated January outgoing longwave radiation. 21

1b. Observed January outgoing longwave radiation. 22

2a. Simulated April outgoing longwave radiation. 23

2b. Observed April outgoing longwave radiation. 24

3a. Simulated July outgoing longwave radiation. 25

3b. Observed July outgoing longwave radiation. 26

4a. Simulated October outgoing longwave radiation. 27

4b. Observed October outgoing longwave radiation. 28

5. Global average outgoing longwave radiation. 30

6. Standard deviation of outgoing longwave radiation. 31

7. Amplitudes for M = 0, N = 2. 33

8. Amplitudes for M = 0, N = 1. 34

9a. January OLR difference (observed-simulated). 39

9b. January t-values. 40

10a. April OLR difference (observed-si mulated). 42

10b. April t-values. 43

11a. July OLR difference (observed-simulated). 44

11b. July t-values. 45

12a. October OLR difference (observed-simulated). 46

12b. October t-values. 47

1. INTRODUCTION

Validation of any general circulation model (GCM) output involves some form of comparison of simulated data versus observed data. In some sense the more accurate and dense our observations are, the more complete our validation can be. However, our knowledge of such basic meteorological parameters as temperature, pressure, and winds is limited due to sparse data, particularly over the oceans. Compounding the validation problem is the accuracy of these data, which may contain some errors as large as 10%.

Fortunately the measurement of at least one atmospheric parameter by our present observation network is both uniformly dense and sufficiently accurate for our purposes. Twice daily measurements of outgoing longwave radiation (OLR) for the past 10 years (June 1974 to May 1984, except March-December 1978) are available on a 2.5 X 2.5 degree global grid. The measurements were made by NOAA satellites. Specific information on the observed OLR data is given in Section 2.

Validation of any model's OLR is really a validation of how well the model simulates the quantities which govern OLR. These include the temperature of the earth-atmosphere system (inherent in this is the temperature of the radiating surface, be it land, sea, ice, or snow), the distribution of cloudiness and the distribution of the major OLR absorbing

and emitting gases (water vapor, ozone, and carbon dioxide). The most important quantities for determining OLR are the distribution and type of clouds. As a simple example, an outbreak of cold air over the central plains of the U.S. would cause a slight decrease in the OLR from that region, while a cloud layer would cause a large reduction in OLR. To date, validation of the OLR field has been unsatisfactory for any general circulation model because virtually all GCM's reproduce the critically important cloud type, amount, and distribution so poorly. However, we feel rapid progress in improvements of GCM's in this area justifies OLR validation.

It seems apparent, then, that a model incorporating some type of cloud interaction capability will yield better results when using OLR as a parameter for validation, than a model without the capability. For this reason we've chosen the GLAS (Goddard Laboratory for Atmospheric Sciences) general circulation model for our study. The model's treatment of cloud-radiation interactions is discussed in detail in Section 3.

The earliest attempts at validation of the output of GCM's, based on zonally averaged data fields and vertical cross-sections of the atmosphere, involved rather qualitative and subjective comparisons. While these comparisons are a useful starting point, a rigorous scientific validation requires more quantitative and objective procedures.

The purpose of this study is to validate with satellite

observations the seasonal variations of OLR simulated by the GLAS model. The data sets are composed of mean annual variations calculated from 9 years of satellite observed OLR and 2 years of OLR simulated by the model. We represent the two data sets as a finite sum of spherical surface harmonics, somewhat along the lines of Christidis and Spar, (1981). This decomposition allows a comparison between the two fields of the annual variations of the amplitudes of the various components and their correlations. A discussion of our application of spherical harmonics is included in section 4. The GLAS model's ability to simulate OLR is evaluated in Section 5 with a variety of comparisons of the simulated vs observed OLR. These include a season-by-season subjective comparison of the two OLR fields, as well as a brief analysis of fields representing differences between the two. Also included are a comparison of the average monthly means and a plot of values calculated using a student's t-statistic.

2. SATELLITE DATA

2.1 Background

NOAA polar orbiting satellites have provided measurements of outgoing longwave radiation (OLR) for approximately 9 years. We now examine the consistency and accuracy of these data to establish their usefulness in GCM validation studies.

The period of observations spans 9 1/2 years, from June 1974 through November 1983, with a 10 month gap during March - December 1978. The remaining nearly 9 years of data have been gathered by seven different satellites. The first four satellites, NOAA 2,3,4, and 5 are members of the NOAA scanning radiometer (NOAA SR) series, and they provided the largest continuous portion of the record (Gruber and Winston, 1978). The 10 month gap began with the failure of NOAA 5 and ended with the launch in January 1979 of the Tiros N satellite. The Tiros N was replaced in February 1980 by NOAA 6 which was succeeded by NOAA 7 in September 1981. These satellites incorporated two important types of changes that affect the homogeneity of our data: 1) different equator crossing times, and 2) different water vapor window channels used for measurement of OLR.

2.2 Equator Crossing Times

Table 1, extracted from a table by Gruber and Krueger

(1984), shows the various satellites and their associated equator crossing times given in local sun time.

Table 1. Equator Crossing Times.

Satellite	Equator Crossing Time
NOAA SR Series	9:00 am and pm
Tiros N	3:30 am and pm
NOAA 6	7:30 am and pm
NOAA 7	2:30 am and pm

Sampling at different times of the day introduces a degree of inhomogeneity into the data record. Gruber and Krueger, (1984) showed that the 12-hour global average OLR difference varies from about 1-2 Wm^{-2} for sunrise/sunset measurements to about 5-6 Wm^{-2} for mid-afternoon/night measurements. From this they infer a diurnal global average OLR cycle having an afternoon maximum and an early morning minimum with an amplitude of about 6-7 Wm^{-2}.

To minimize the effect of the diurnal variation on the record the average of the two daily measurements is used. A comparison of the zonal profiles of averaged annual OLR measured by each satellite shows only small differences (Gruber and Krueger, 1984). Gruber and Krueger point out that these differences, on the order of a few Wm^{-2}, may be attributable in large part to inter-annual variability of

the OLR, and do not detract significantly from the assumption of homogeneity in the data.

2.3 Procedures

The original NOAA SR series window channel spanned the region from 10.5 to 12.5 μm. On Tiros N and NOAA 6 the window channel was narrowed to 10.5 to 11.5 μm, while on NOAA 7 the infrared channel used for OLR measurements covered 11.5 to 12.5 μm (Janowiak et al., 1985).

In addition to variations in the window channel, another factor that went through several modifications was the algorithm used to derive total OLR from observations in a narrow band. Nark et al., (1962) found the relationship between the narrow band measurement and total outgoing longwave emittance to be linear in a sample of 99 different atmospheres. This linear relationship was used on data gathered by the NOAA SR series of satellites. Then, Abel and Gruber (1979) showed that a non-linear algorithm provided a better fit. Their relation was used to convert the entire record then existent. Versions of this new non-linear relation were used for the data collected by the different window channels of the Tiros N and NOAA 6 satellites.

However, Ellingson and Ferraro (1983) in comparing fluxes from the NOAA satellites with observations from the NIMBUS 6 Earth Radiation Budget experiment found through their radiance calculations that, except for clouds below 750 mb, the relationship derived by Abel and Gruber over-

estimated the OLR from partial cloud cover. The magnitude of the errors varied with cloud type and amount but in some cases was as large as 2% of the planetary outgoing flux. The subsequent NOAA 7 data used an updated algorithm based on the work of Ellingson and Ferraro.

Finally, Ohring et al. (1984) reviewed the procedure for converting window measurements to total OLR and found that the record based on the previous methods contained a positive bias of about 13 Wm^{-2}. Their work involved an analysis of simultaneous measurements from the NIMBUS 7 satellite of the total longwave emittance and the radiance in the 10-12 μm window measured by the Thermal Infrared Radiometer (THIR). The new algorithm developed by Gruber and Krueger reduced the global average OLR by approximately 11 Wm^{-2} (Gruber and Krueger, 1984). By relating the THIR window radiance to the window radiances of each of the satellites participating in this data collection, Gruber and Krueger, (1984) also derived appropriate algorithms to enable a final update of the entire record.

Because of the extensive work and multiple refinements in the algorithms that calculate total OLR from window measurements described above, we believe the data set to be a good representation of the actual total OLR field.

3. THE GLAS MODEL

3.1 Model Description

The version of the GLAS model used in this study is based on the Goddard Institute for Space Studies (GISS) general circulation model. The GISS model, described by Somerville, et al. (1974) was used to a large extent in support of the Global Atmospheric Research Program (GARP) and had evolved from the 3-level GCM developed at UCLA by A. Arakawa and Y. Mintz (Arakawa, 1972).

The GLAS GCM is a 9-level primitive equation model in sigma coordinates. Each of the nine vertical levels has the same sigma thickness. The total mass of the model atmosphere, which in pressure units is surface pressure minus pressure at the top, is divided into nine equal layers. The upper boundary of layer 1 is at 10 mb. A vertical differencing scheme is employed based on the work of Arakawa and Lamb (1977) and Arakawa and Suarez (1983). Horizontal grid spacing is four degrees of latitude by five degrees of longitude. Variables are horizontally staggered according to the B-grid scheme of Arakawa and Lamb (1977). To maintain computational stability, selected fields are filtered in the longitudinal direction near the poles with a Fourier filter based also on the design of Arakawa and Lamb (1977). The Fourier filter is applied to the zonal wind, which is used to compute the zonal mass flux, and to the zonal component

of the pressure gradient force.

A recently modified planetary boundary layer (PBL) parameterization (Randall, 1982a) has been included which incorporates an improved surface flux parameterization. However, even with these improvements the model simulates planetary albedo as 0.40 compared with an observed planetary albedo of approximately 0.30 (Shukla et al., 1981).

The GLAS model contains sophisticated routines for dealing with radiation in both clear and cloudy skies over the entire spectral range. However, since this study focuses on the outgoing longwave radiation, only the model's treatment of longwave radiation will be addressed.

3.2 Longwave Radiation

The most important absorbers of longwave radiation in the atmosphere are water vapor, carbon dioxide, and ozone. The GLAS model uses the Wu-Kaplan radiation routine (Krishnamurthy, 1982), which is summarized here, in its treatment of these absorbers.

3.2.1 Absorbers

The absorption of radiation by atmospheric gases is spectrally dependent. The spectral region where the absorption occurs is determined by the molecular structure of the gases. Radiation is absorbed in spectral bands which consist of many individual narrow lines. Water vapor has a strong vibration-rotation band at 6.3 μm and pure rotation

bands at wavelengths greater than 20 μm. In the Wu-Kaplan radiation routine, the temperature dependence of absorption coefficients in the 6.3 μm water vapor vibration-rotation band is not taken into account, as the radiative transfer in that band is relatively small. The most important carbon dioxide band is a vibration-rotation band at 14.7 μm, while ozone absorbs intensely near 9.6 μm with other bands at 4.7 μm and 14.1 μm. In the regions between the molecular absorption bands, atmospheric gases are relatively transparent. However, water vapor has an absorption continuum in the atmospheric window region between approximately 8 μm and 13 μm.

3.2.2 Transmission Functions

Of the three major absorbers, detailed calculations are carried out for water vapor only, while pre-calculated quantities such as transmission functions are used for carbon dioxide and ozone. Because of the complicated structure of the spectral absorbing bands, it is a formidable task to carry out a line-by-line integration of the transmission functions. Therefore it is necessary to make some reasonable approximations to compute transmission functions.

The apparently random line positions of the absorbing gases in the absorption spectra make it possible to treat absorption in a band statistically. Goody (1952, 1964) found that a simple Poisson distribution of line strengths agrees well with experimental water vapor data. Another

very useful approximation makes it unnecessary to integrate over exact line shapes, which change with pressure and in variations of amount of absorber. The Curtis-Godson approximation states that transmission along a non-homogeneous path is very close to that along a path at constant pressure with a constant effective absorber amount. As a result, a single line absorbing along a non-homogeneous path can be closely represented by a line absorbing along a homogeneous path by adjusting the line intensity and width. Choice of width and intensity is made to give correct absorption in the weak- and strong-line limits. Following the work of Elsasser (1942) and Rodgers and Walshaw (1966) in approximating the flux transmission function, a diffusivity factor of 1.66 has been included.

Mean transmission functions used for carbon dioxide were pre-calculated line-by-line by Dr Virgil Kunde of the NASA Goddard Space Flight Center (Krishnamurthy, 1982) based on an assumed standard temperature sounding and a uniform mixing ratio of CO_2. The transmission functions used for ozone were pre-calculated by Dr Noelle Scott of the Laboratoire de Meteorologie, Paris (Krishnamurthy, 1982). The multiplicative property of transmission functions is used in case of overlap of absorption spectra of different absorbers in a particular spectral interval.

3.2.3 Clouds

Clouds occur if the model predicts large-scale super-

saturation, which consists of a comparison at each grid point of the saturation and actual mixing ratios. When clouds occur an iterative reduction of the mixing ratio (accompanied by a rise in temperature due to latent heat release) is carried our until the relative humidity at the grid point equals 100%. Clouds are also created when a specific type of comparison of pairs of layers shows the lower layer to be buoyant with respect to the higher layer. These convective clouds are assumed to fill an entire horizontal grid box. However, since 100% fractional cumulus cloudiness is unrealistic, radiation effects of convective clouds are neglected by the model. This actually leads to an improved longwave radiation distribution (Moeng and Randall, 1982). Clouds are assumed to be black bodies, however, to alleviate excessive cooling due to high-level clouds in the model, all clouds in the top three layers of the model are considered to be transparent with respect to radiation. Latent heating and drying due to large-scale super-saturation in these three layers still occur. All condensate released is assumed to precipitate to the next lower unsaturated layer where it evaporates. A cloud is created wherever condensation raises the relative humidity to 100%. Each column of layers is tested from the top downward, and condensation in layer 9 precipitates.

3.2.4 Longwave Flux

A given volume of atmosphere both receives and emits

infrared (longwave) radiation and warms or cools according to the net vertical flux across the volume. In computing longwave vertical fluxes, the Wu-Kaplan radiation routine considers the following absorbers and their associated absorption regions:

(1) Water vapor (0 - 2050 cm^{-1}),
(2) Water dimer (660 - 1200 cm^{-1}),
(3) Carbon dioxide (500 - 800 cm^{-1}),
(4) Ozone (800 - 1200 cm^{-1}).

Parameters used to compute longwave fluxes at each grid point are pressures, temperatures, specific humidities and cloud status at all vertical levels, as well as latitude, number of spectral intervals, Julian day, and pre-calculated transmission functions. For purposes of radiation flux calculations, two stratospheric layers, with upper boundaries at 1 mb and 5 mb, are added to the nine tropospheric layers. Temperatures at the tops of these two stratospheric levels come from the climatological data of Newell, et al. (1974). In addition, each original model layer is divided into two "radiation" layers to enhance calculation accuracy. Transmission functions and Planck functions are computed at the 19 radiation levels. Use of Simpson's three-point rule, which requires temperature and specific humidity values midway between radiation levels, requires that each radiation layer be further divided into two "radiation sublay-

ers". Net longwave fluxes are computed at the upper boundaries of all model layers and at the lower boundary of the bottom (9th) layer. Specific details on numerical techniques involved in computing fluxes are described in Wu (1976).

3.2.5 Initialization

The GLAS model was initialized with the observed atmospheric conditions of 15 November, 1978. Prescribed boundary conditions included topography and climatological values of sea surface temperatures, surface albedoes, and snow/ice distributions. Initial soil moistures were calculated from climatological values of surface relative humidities (Randall, 1982).

4. Spherical Harmonics

One tool for objectively describing the GLAS model's skill in simulating OLR is the spherical harmonic method of analysis which Christidis and Spar (1981) call "a valuable critical tool for comparing synoptic patterns and evaluating the output of general circulation models."

4.1 Properties of Spherical Harmonics

We can express F, our OLR data field (a function of latitude and longitude) as a sum of terms as follows:

$$F(\theta,\phi) = \sum_{n=0}^{N} A_n P_n(\mu) + \sum_{m=1}^{N-1} \sum_{n=m}^{N} 2 \left[A_{n,m}\cos(m\phi) - B_{n,m}\sin(m\phi) \right] P_{n,m}(\mu) \quad (1)$$

Where (see Byerly, 1893, and Blackmon, 1976):

θ = co-latitude (90 minus latitude in degrees)

ϕ = longitude

$\mu = \cos\theta$

m = number of waves around a latitude circle; order of the harmonic

n = degree of the harmonic

n-m = number of zero points between poles

$n \geq m$ in all cases

$P_n(\mu)$ = Legendre polynomial, or zonal harmonic defined as follows:

$$P_n(\mu) = \frac{1}{2^n n!}\frac{d^n(\mu^2-1)^n}{d\mu^n} \qquad \text{(Rodrigue's formula)}$$

and,

$P_{n,m}(\mu)$ = Associated Legendre function defined as follows.

$$P_{n,m}(\mu) = (1-\mu^2)^{m/2}\frac{d^m}{d\mu^m}P_n(\mu)$$

The expansion (1) is based on the orthogonality conditions:

For Legendre polynomials,

$$\int_{-1}^{1} P_m(\mu)P_n(\mu)d\mu = 0 , \quad n \neq m$$

and,

$$\frac{2n+1}{2}\int_{-1}^{1} [\,P_n(\mu)\,]^2\,d\mu = 1$$

Likewise for associated Legendre functions,

$$\int_{-1}^{1} P_{n,m}(\mu)P_{k,m}(\mu)d\mu = 0 , \quad n \neq k$$

and,

$$H\int_{-1}^{1} [\,P_{n,m}(\mu)\,]^2\,d\mu = 1$$

with $H = \frac{(2n+1)(n-m)!}{(n+m)!}$

(A_n, $A_{n,m}$) and ($B_{n,m}$) are the expansion coefficients of the series where,

$$A_n = J \int_0^{2\pi} \int_{-1}^{1} F(\theta,\phi) P_n(\mu)\, d\mu\, d\phi$$

with $J = \frac{2n+1}{\pi}$;

$$A_{n,m} = K \int_0^{2\pi} \int_{-1}^{1} F(\theta,\phi) P_{n,m}(\mu) \cos(m\phi)\, d\mu\, d\phi$$

$$B_{n,m} = K \int_0^{2\pi} \int_{-1}^{1} F(\theta,\phi) P_{n,m}(\mu) \sin(m\phi)\, d\mu\, d\phi$$

with $K = \frac{(2n+1)(n-m)!}{\pi\ (n+m)!}$.

4.2 Application

In the series (1) explained variance of the field F increases as N increases. However, in using a modification of computer routines based on code supplied by Dr Jordan Alpert of NASA, (private communication) we find that truncating at N = 7 (triangular truncation), captures approximately 90% of the variance of the original fields. For greater accuracy we've chosen to truncate at N = 15, enabling us to reconstruct OLR fields which explain at least 96% of the variance of the original fields.

Since our two data sets have different grid sizes, they are not directly comparable for some applications. To be fair to the model with its coarser grid, all fields of observed OLR have been decomposed into spherical harmonics and recomposed onto the same 4 X 5 degree grid as the model's fields. Specifically, the global average observed OLR field for a given month was calculated by averaging n years of observed data for that month, point by point, to get an average field. This average field was then decomposed and reconstructed onto the coarser grid. Calculation of the observed field's average standard deviation involved decomposing and reconstructing each of the observed months (9 January's, for example) prior to the appropriate point by point summations over the n years.

After representing both data sets on the same grid scale by a sum of spherical harmonic components, we can look at two different aspects in our comparison of these components. The amplitude of a component gives us a measure of how much of the variance of the total field is explained by that component. Likewise, the agreement of the phases of the same components in each data set gives us correlation coefficients relating the two fields. The amplitude and phase of the n,mth harmonic are given as follows:

$$(AMP_{n,m})^2 = (A_{n,m})^2 + (B_{n,m})^2$$

$$(PHASE_{n,m}) = \tan^{-1}(B_{n,m}/A_{n,m})$$

Calculation of correlation coefficients and explained variances by component are described in Appendix I. Tables of amplitudes and explained variances by wave number are given in Appendices II and III.

5. Analysis and Results

In all comparisons presented here, simulated data represents the average by month of two annual cycles (i.e, two January's, two February's, etc) produced by the GLAS model. Each month of observed data shown is the average of nine years of that month, except for February and May which had ten and eight years respectively.

We begin with subjective comparisons of simulated vs observed data for the four seasons. Figures 1a and 1b show average January OLR, simulated and observed. The gross features of higher OLR values at low latitudes and lower values a high latitudes are reproduced by the model. The most striking difference between the two fields is in the magnitude of OLR. In most places simulated OLR is considerably lower than observed. Also note the stronger north-south gradient of simulated OLR at mid-latitudes of both hemispheres. Finally, the model seems to show less longitudinal structure in general than observations.

Figures 2a and 2b through 4a and 4b, which represent simulated and observed fields for April, July, and October show similar disagreements. The model seems to underestimate OLR the most at high latitudes and to reproduce it most closely in the lower latitudes. The only areas where the model overestimates OLR are in three areas of the tropics: central Africa, Indonesia/Southeast Asia, and along the

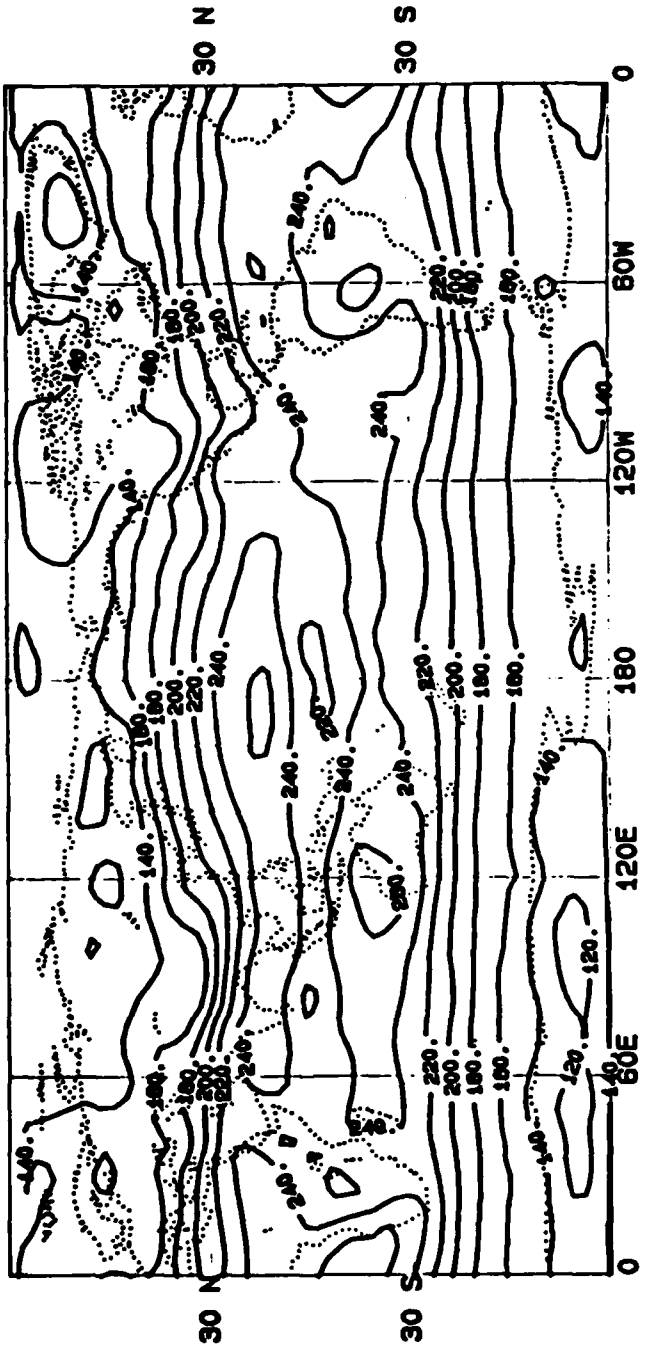

Figure 1a. Simulated January outgoing longwave radiation.

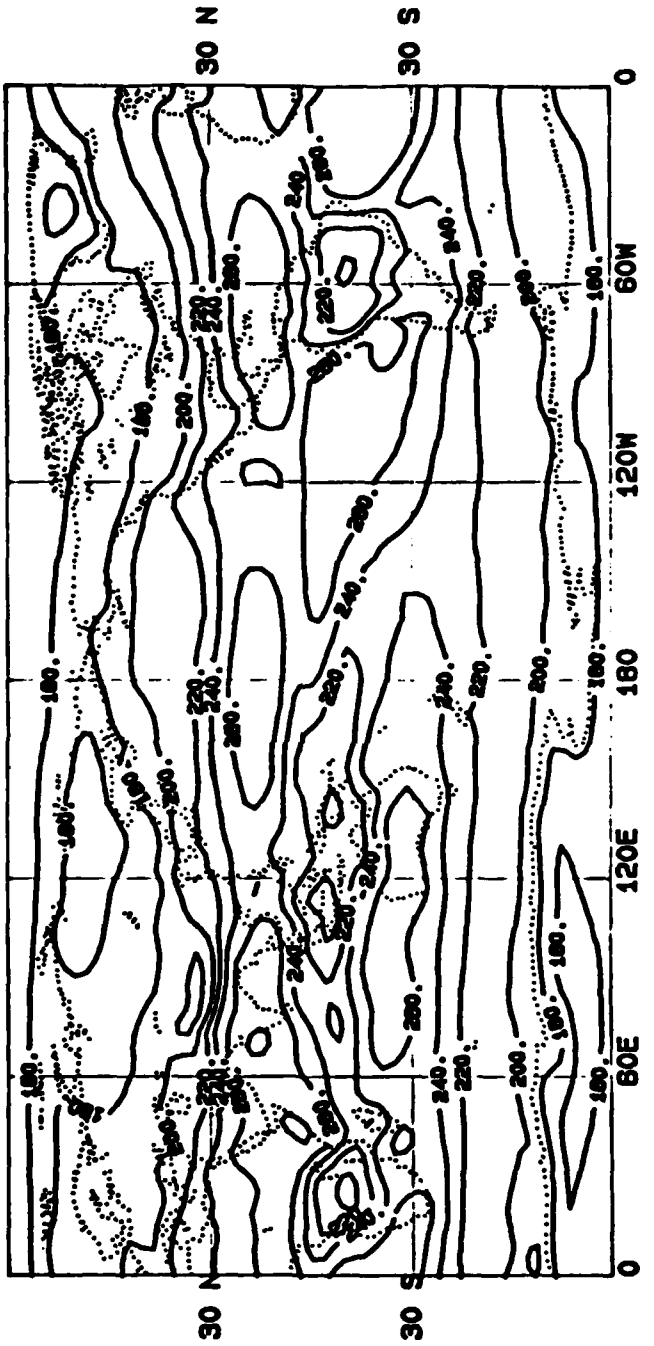

Figure 1b. Observed January outgoing longwave radiation.

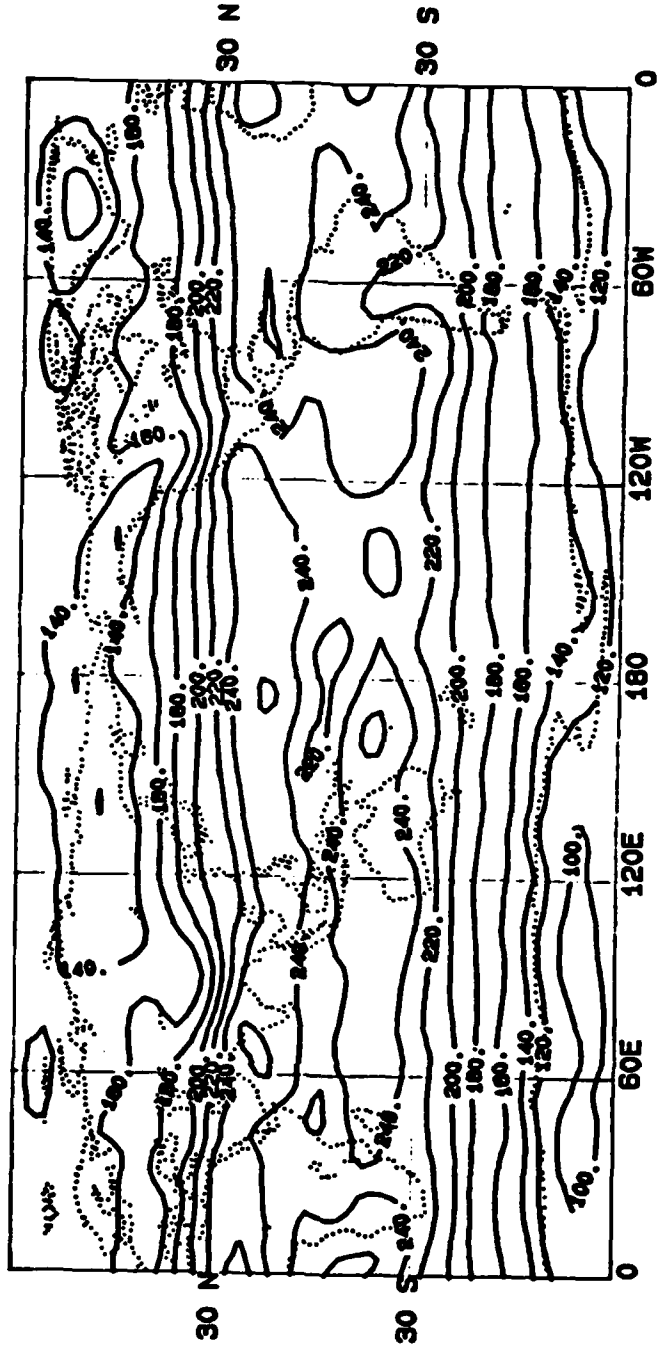

Figure 2a. Simulated April outgoing longwave radiation.

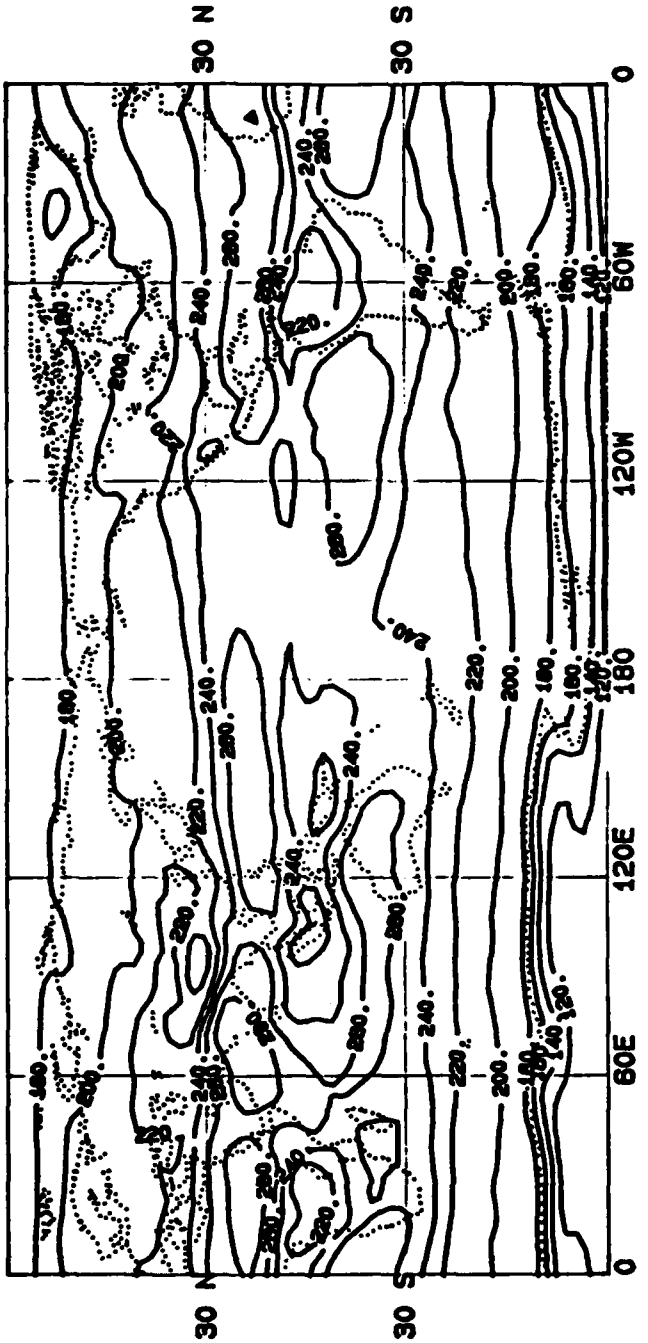

Figure 2b. Observed April outgoing longwave radiation.

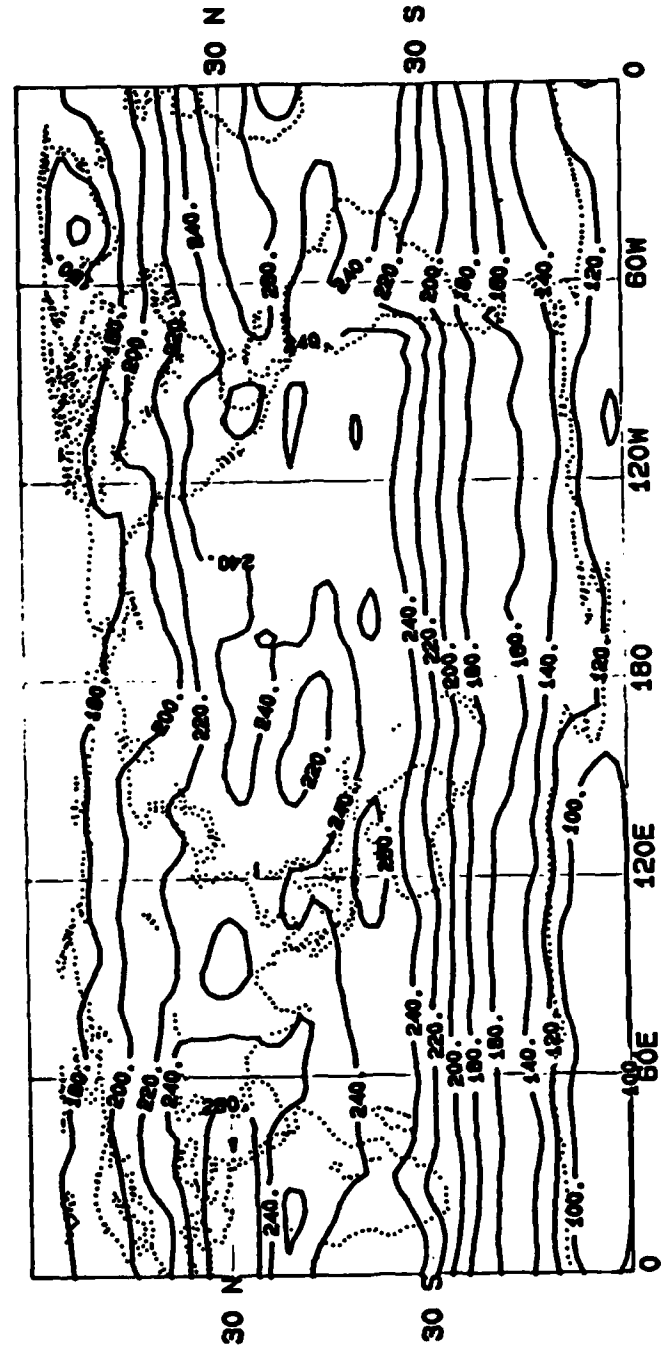

Figure 3a. Simulated July outgoing longwave radiation.

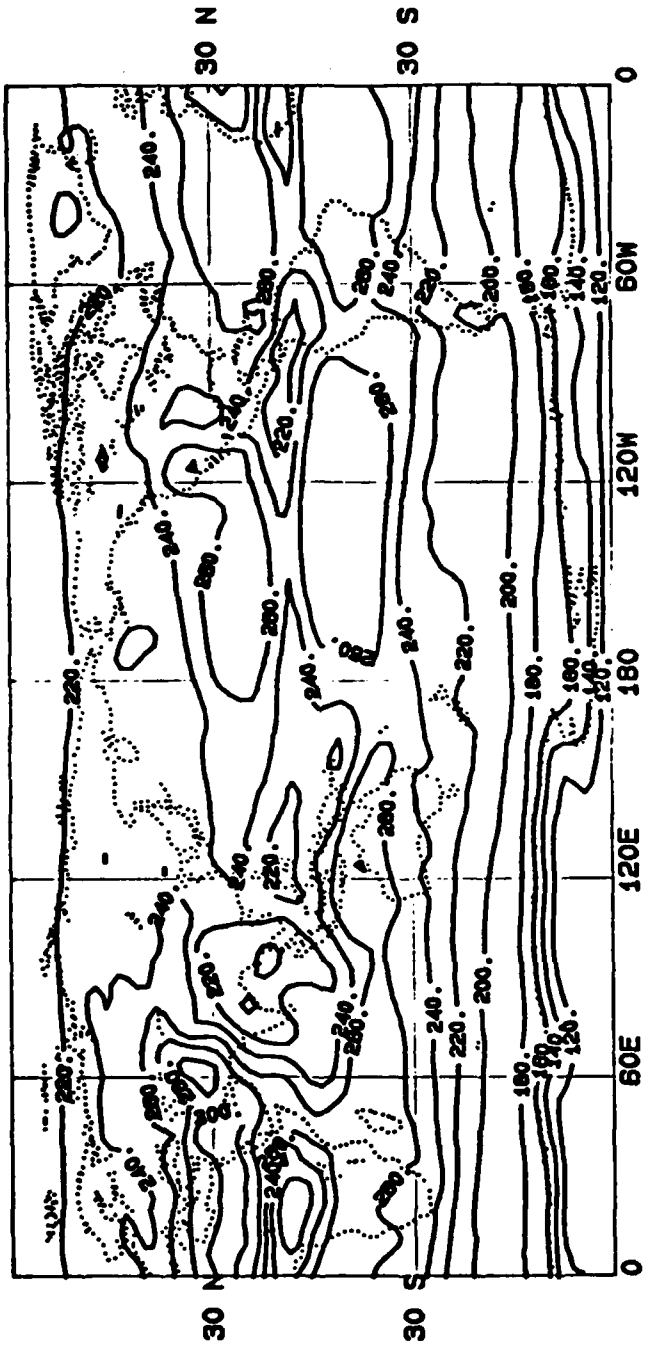

Figure 3b. Observed July outgoing longwave radiation.

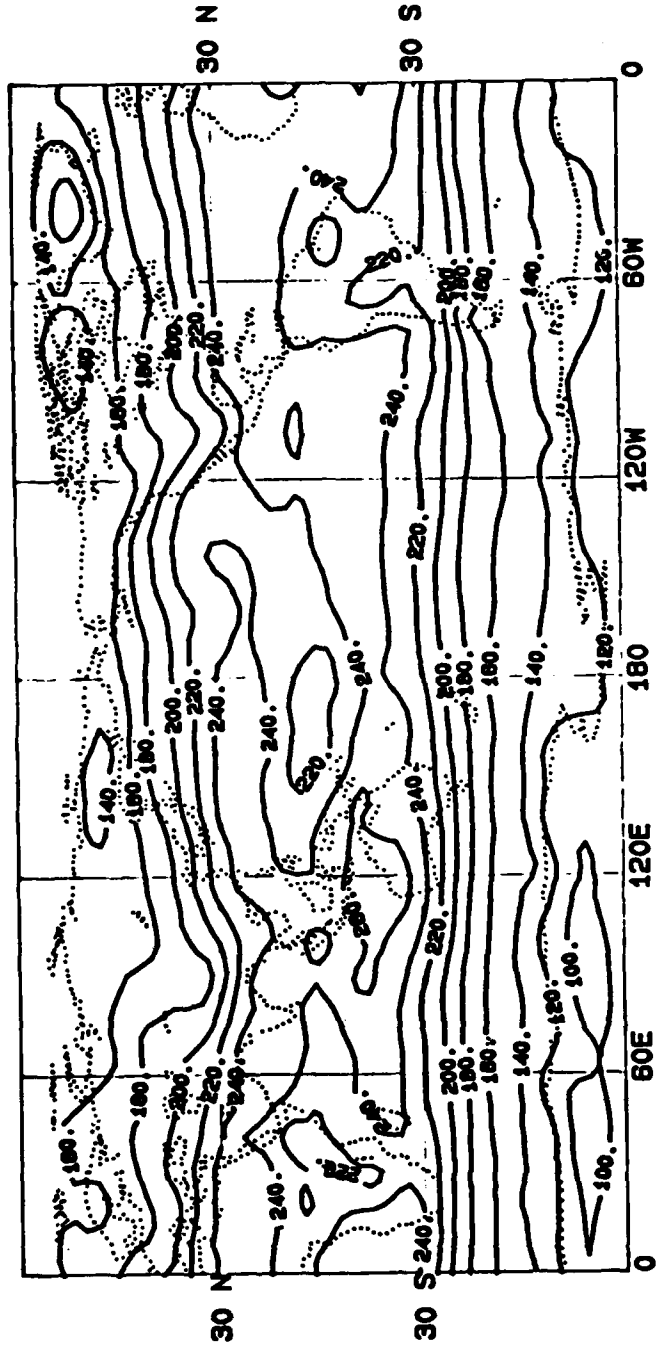

Figure 4a. Simulated October outgoing longwave radiation.

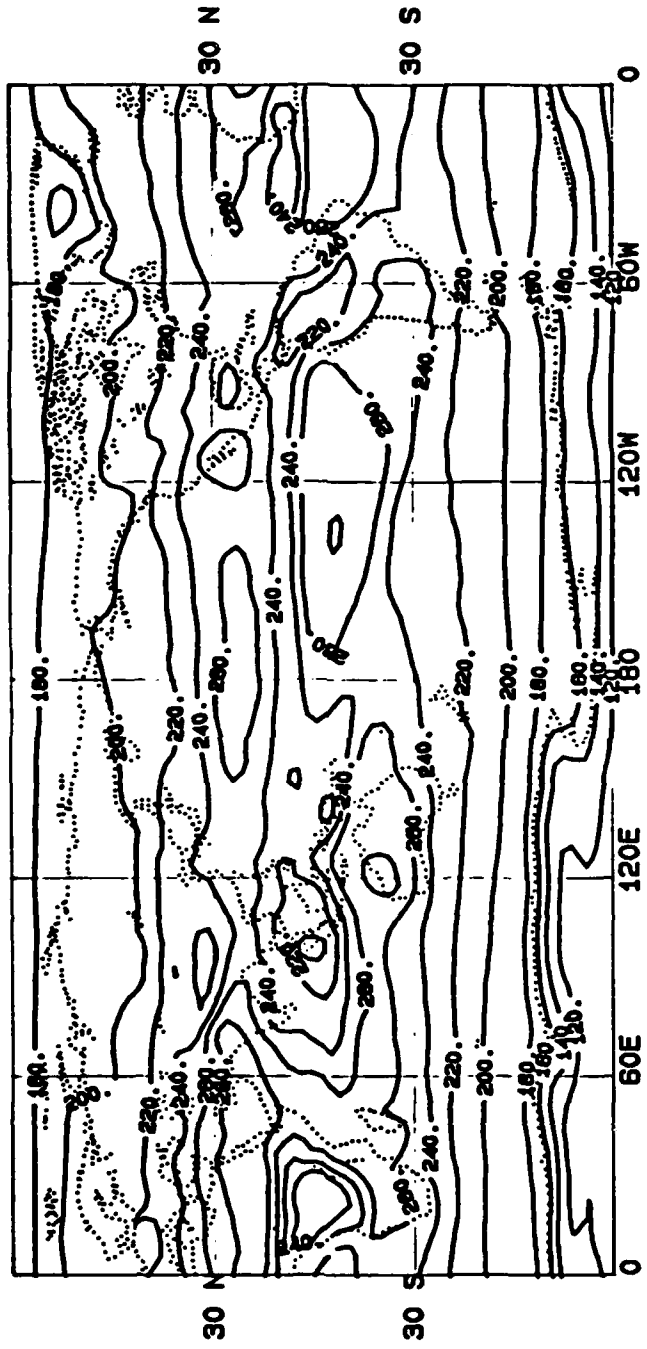

Figure 4b. Observed October outgoing longwave radiation.

Amazon River in S. America. These areas are well known regions of convective activity and, since the GLAS model does not allow convective clouds to interact with radiation, it fails to appropriately reduce the OLR here.

These qualitative comparisons give us a general idea of how well the model simulates OLR but we have another means of comparison which is less subjective than a simple visual comparison and which gives us further insight into how and why the model's simulation differs from observations. In Section 4 we discussed how spherical harmonics could be used to break a field down into components. We now use those methods to compare some of the major components of the two data sets.

We know from Figures 1a-1b through 4a-4b that, in general, simulated OLR is too low. Figure 5 shows that the magnitude of the difference in global averages is about 20-23 Wm^{-2} throughout the year. We also see that the model performs fairly well in simulating the observed seasonal cycle of average OLR with higher values in the (northern hemisphere) summer and lower values in winter. Figure 6 shows that, to a lesser degree, the model also successfully simulates the seasonal pattern of variation of standard deviation of the geographical field. Simulated standard deviation values range from about 8-12 Wm^{-2} higher than observed.

Appendix II shows the amplitudes of all spherical harmonic components (truncated at N = 15) for the four seasons, both observed and simulated. For each month the spherical

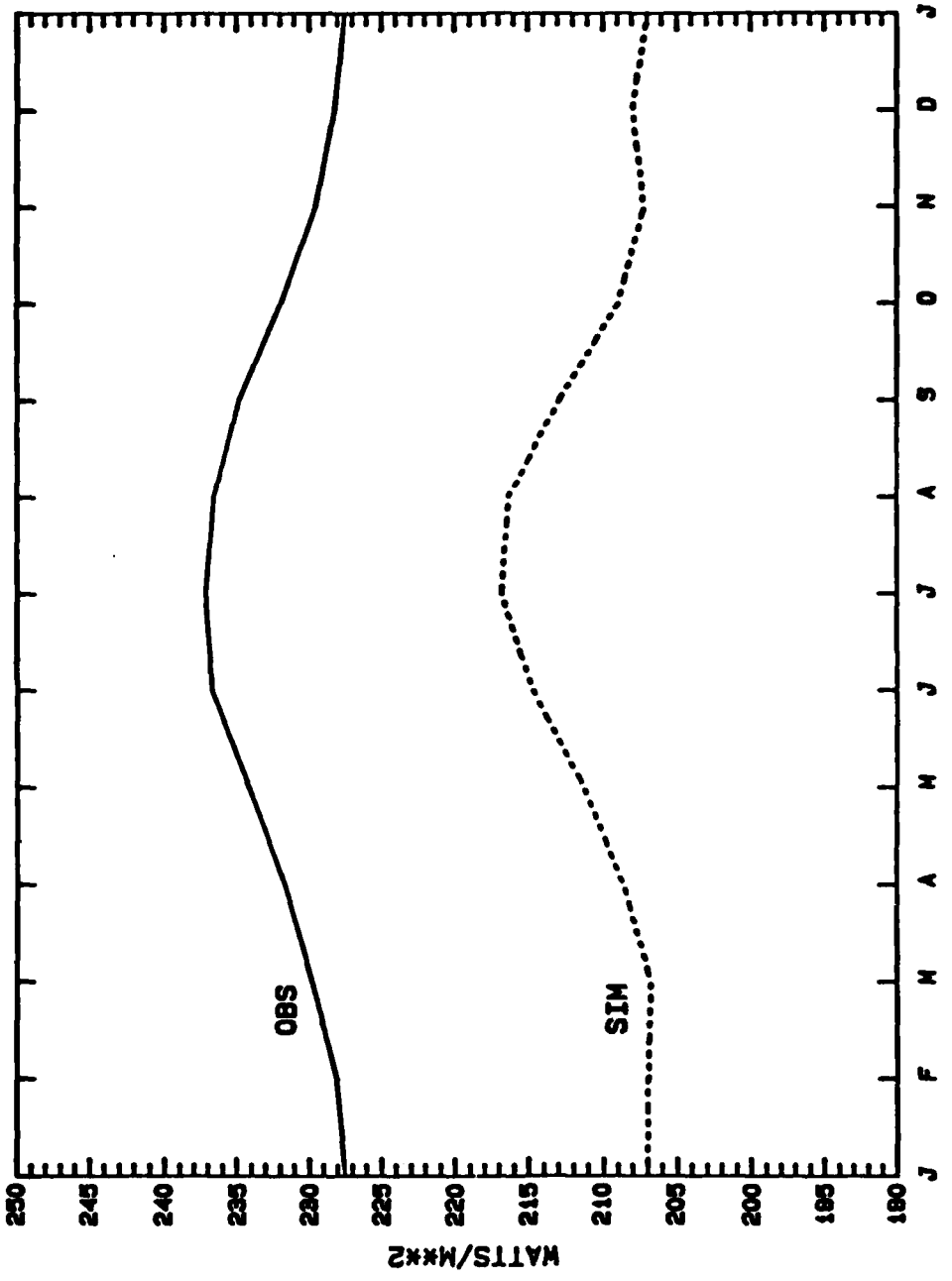

Figure 5. Global average outgoing longwave radiation.

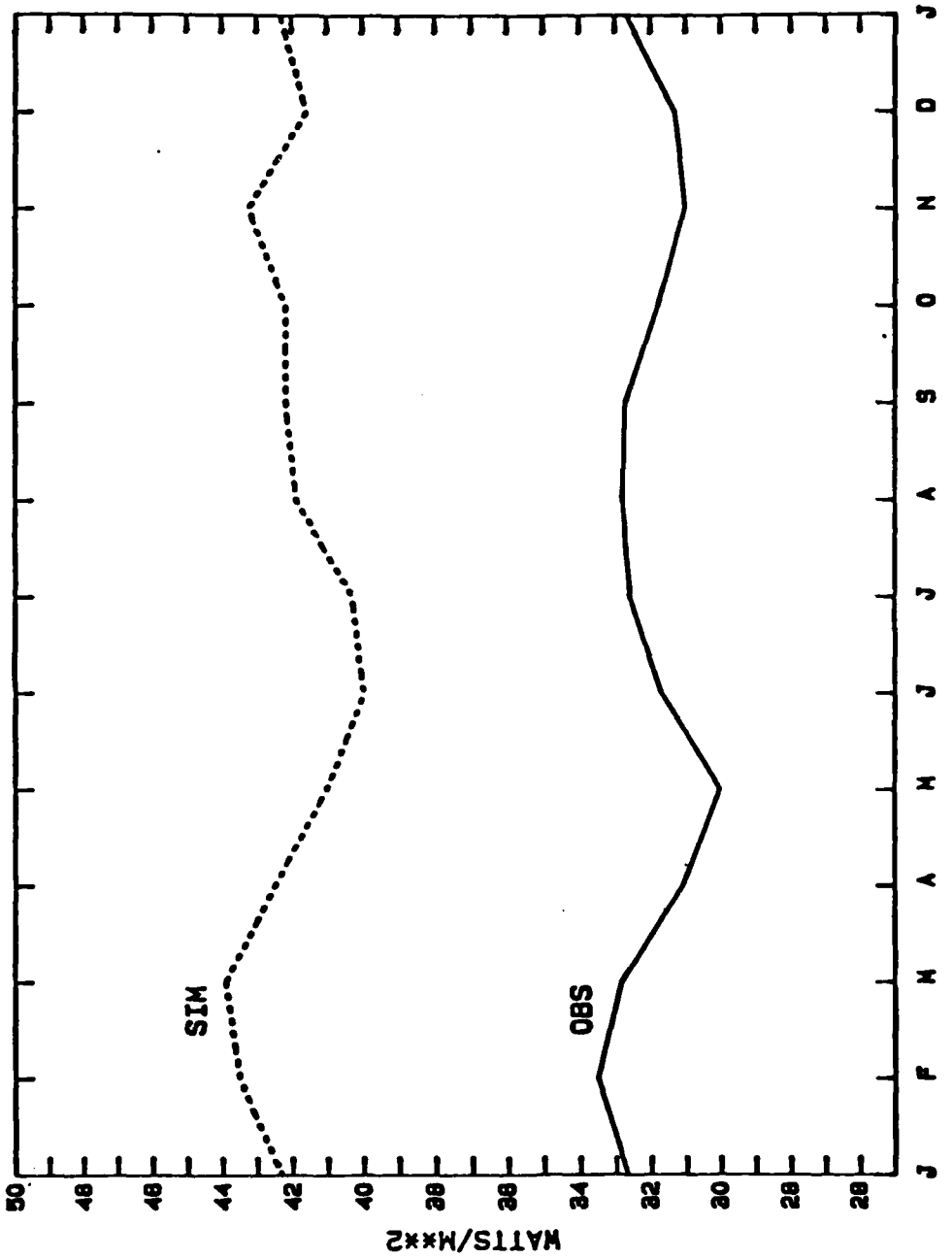

Figure 6. Standard deviation of outgoing longwave radiation.

harmonic component corresponding to the symmetric part of wave number 2 (N = 2, M = 0) is by far the dominant one. This component is a major contributor to the spatial variability of the OLR field and is also symmetric about the equator, and provides a measure of the annual average. It explains as much as 2/3 of the total variance of the observed OLR field (see Appendix III for explained variances by component). The model, however, places even more emphasis on this component, using it to explain as much as 4/5 of the total variance of the simulated field. Figure 7 shows a plot of the simulated and observed N = 2, M = 0 component amplitudes by month. We see that the amplitude of the simulated component is about 12 Wm^{-2} too high throughout the year. On the other hand, the seasonal pattern is reproduced fairly well.

The next most dominant component corresponds to N = 1, M = 0. It is the dominant mode of seasonal variation being antisymmetric about the equator, and its amplitudes are shown in Figure 8. As in Figure 7, the model adheres well to the observed seasonal pattern. However, the magnitudes of simulated amplitudes are much more realistic here, being too high by as much as 6 Wm^{-2} only in the (northern hemisphere) summer and in relative agreement the rest of the year.

Having examined dominant component amplitudes, we turn our attention to the agreement between the phases of the observed and simulated OLR components. Just as explained

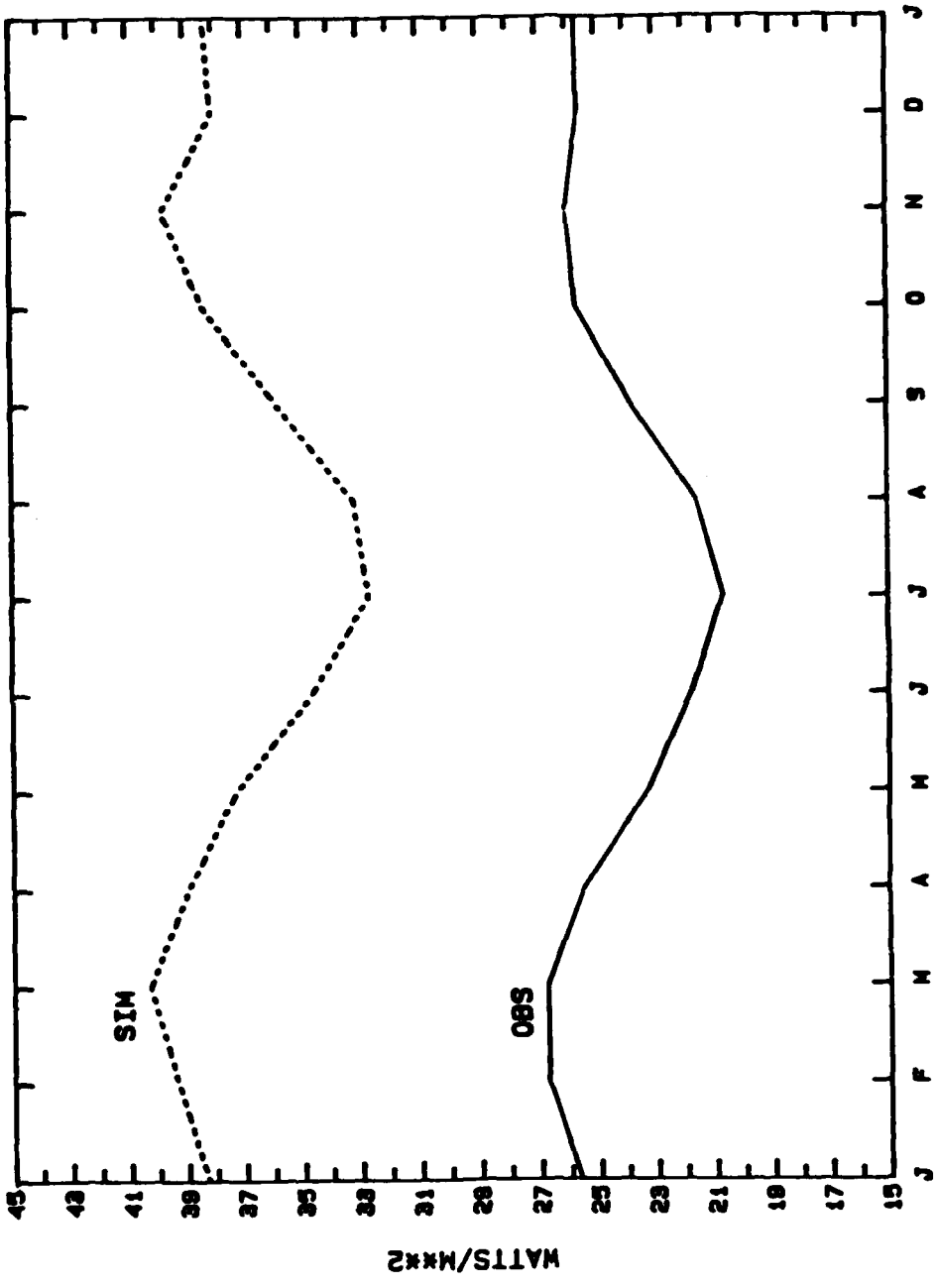

Figure 7. Amplitudes for M = 0, N = 2.

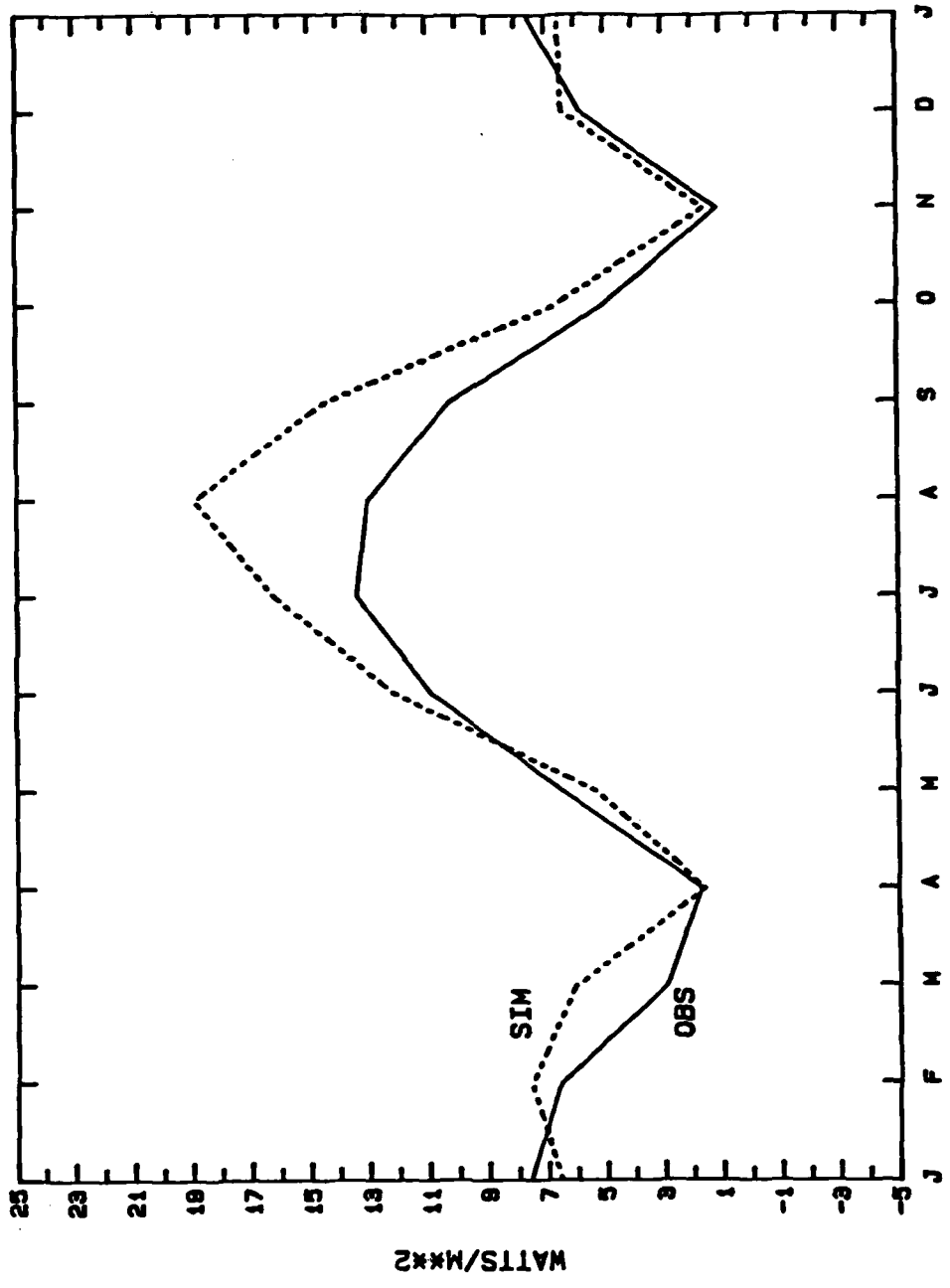

Figure 8. Amplitudes for M = 0, N = 1.

variance was used as a measure of agreement between amplitudes, we can use correlation coefficients to measure the association between the phases of observed and simulated fields as a function of spatial scales.

Tables 2-3 show correlation coefficients for wave numbers 1 through 15 broken down into symmetric and asymmetric components. The symmetric part, which corresponds to spherical harmonic components with M = 0, (i.e. the zonally averaged component) describes how well the north-south variability of the two fields agree in phase. The asymmetric parts ($M \neq 0$) measure the agreement of east-west variability (i.e. the departure from zonal average) between the phases of the observed and simulated fields. The tables are cumulative in that the values for N = 5, for example, represent a comparison not of wavenumber 5 phases alone, but of how well the phases of the two data sets for waves 1 through 5 agree. The very high symmetric component correlations indicate that the model does an excellent job of simulating the phases of the zonal OLR features. The phases of the longitudinal features of OLR are less accurately reproduced by the model, as shown by the low asymmetric component correlations. It is interesting to note that when all 15 waves are considered, the total correlation coefficients and the symmetric component coefficients remain nearly constant across the seasons, while the asymmetric correlation coefficients are considerably lower during April and October than in January and July. A look at the variances in Appendix III shows that a

Table 2. January and April Correlation Coefficients

JANUARY

N	CORRELATION COEFFICIENT	SYMMETRIC COMPONENT	ASYMMETRIC COMPONENT
1	0.97	1.00	0.93
2	0.97	0.99	0.09
3	0.96	0.99	0.37
4	0.95	0.98	0.55
5	0.94	0.97	0.55
6	0.93	0.97	0.55
7	0.92	0.97	0.54
8	0.91	0.96	0.51
9	0.91	0.96	0.52
10	0.90	0.96	0.53
11	0.90	0.96	0.53
12	0.90	0.96	0.53
13	0.90	0.96	0.52
14	0.90	0.96	0.52
15	0.90	0.96	0.52

APRIL

N	CORRELATION COEFFICIENT	SYMMETRIC COMPONENT	ASYMMETRIC COMPONENT
1	0.14	-1.00	0.81
2	0.98	0.99	0.45
3	0.98	0.99	0.51
4	0.96	0.98	0.58
5	0.96	0.98	0.59
6	0.95	0.98	0.56
7	0.94	0.97	0.50
8	0.93	0.97	0.48
9	0.92	0.97	0.49
10	0.92	0.96	0.49
11	0.91	0.96	0.47
12	0.91	0.96	0.47
13	0.91	0.96	0.45
14	0.91	0.96	0.46
15	0.91	0.96	0.45

Table 3. July and October Correlation Coefficients

JULY

N	CORRELATION COEFFICIENT	SYMMETRIC COMPONENT	ASYMMETRIC COMPONENT
1	0.99	1.00	0.99
2	0.97	0.99	0.88
3	0.95	0.97	0.77
4	0.93	0.97	0.73
5	0.93	0.97	0.75
6	0.92	0.97	0.74
7	0.92	0.96	0.73
8	0.91	0.96	0.72
9	0.91	0.96	0.71
10	0.91	0.96	0.71
11	0.90	0.96	0.69
12	0.90	0.96	0.69
13	0.90	0.95	0.68
14	0.90	0.95	0.68
15	0.90	0.95	0.67

OCTOBER

N	CORRELATION COEFFICIENT	SYMMETRIC COMPONENT	ASYMMETRIC COMPONENT
1	0.98	1.00	0.84
2	0.98	1.00	0.24
3	0.97	1.00	0.31
4	0.95	0.98	0.32
5	0.94	0.98	0.37
6	0.93	0.98	0.39
7	0.92	0.98	0.40
8	0.92	0.98	0.40
9	0.91	0.97	0.42
10	0.91	0.97	0.42
11	0.91	0.97	0.40
12	0.90	0.97	0.39
13	0.90	0.97	0.38
14	0.90	0.97	0.37
15	0.90	0.97	0.37

similar feature occurs in the amplitudes. During April and October, both the model and observations show a decrease in the variance explained by the amplitudes of asymmetric components.

Finally, we present the results based on the student's 't' statistic. Figure 9a shows the difference between observed and simulated OLR for January. We saw in Figures 1a and 1b that in most areas simulated OLR values were lower than observed values. Figure 9a makes it much easier to see that the model errors for January range from 60 Wm^{-2} too low at some high southern latitudes and along northwestern N. America to as much as 45 Wm^{-2} too high at the three areas of convective activity in the tropics. While these numbers are useful in themselves, they become much more so if we know whether or not they are statistically significant.

Figure 9b shows the field of values calculated using a student's t-statistic (see Appendix I for calculations of t-values). We use these values to test the null hypothesis that the difference between simulated and observed OLR means are not significantly different from zero. The heavy solid contour, 2.3, and the heavy dashed contour, -2.3, represent the boundaries of areas of significance at the .05 level for a two-tailed test. Areas with values between +2.3 and -2.3 (i.e. areas inside the 2.3 contour but outside the -2.3 contour are the only areas where the means of the two data sets are <u>not</u> significantly different. From Figure 9b, then, we see that nearly all values outside the tropics are

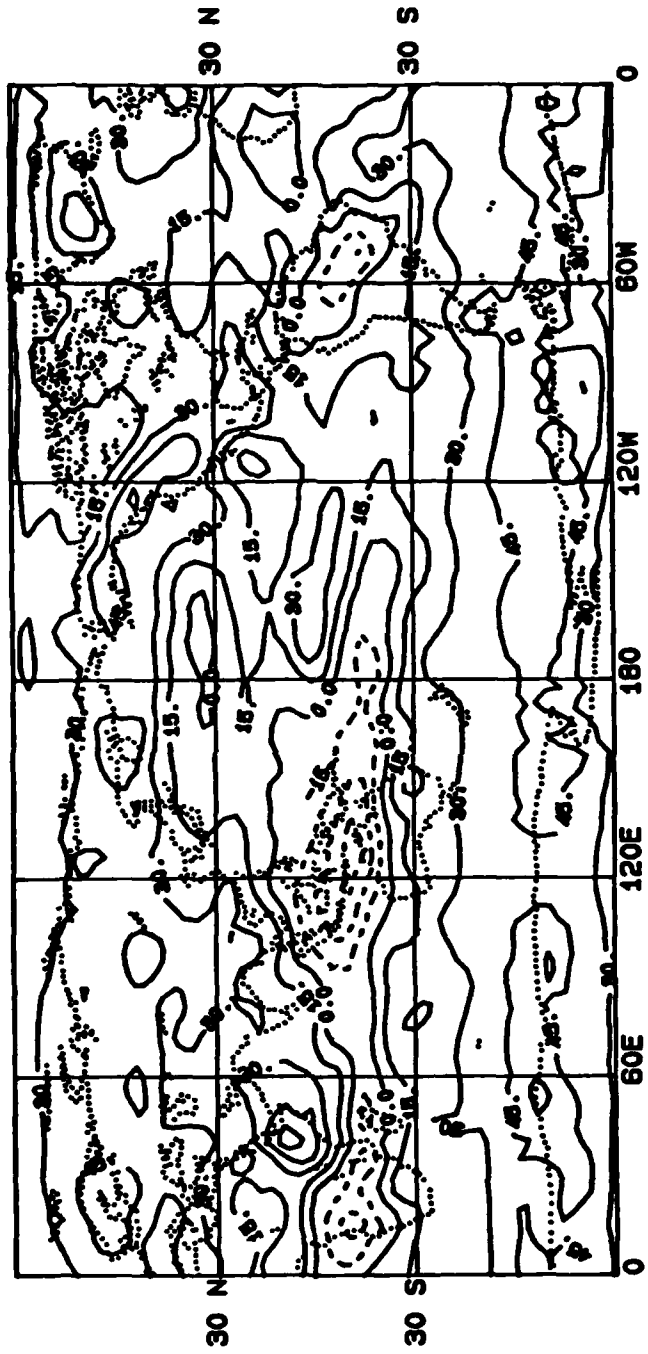

Figure 9a. January OLR difference (observed - simulated).

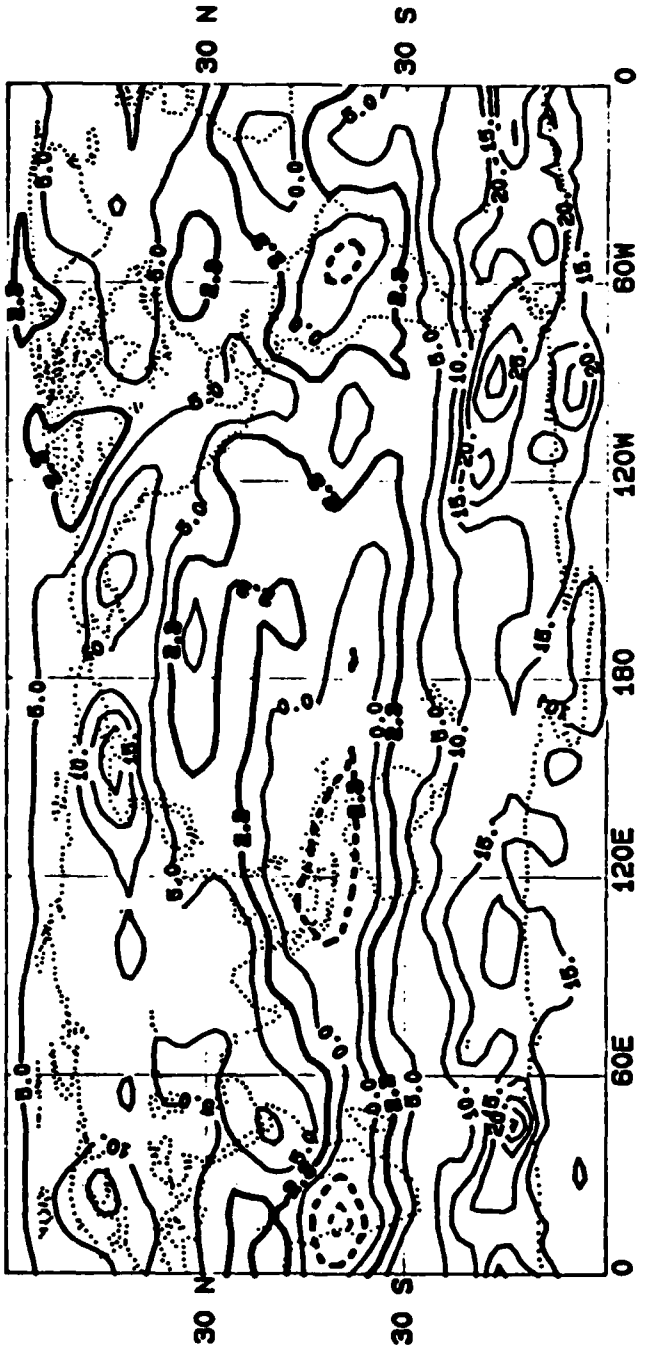

Figure 9b. January t-values.

statistically significant and values in the three convective centers within the tropics are also statistically significant. Let us now advance through the seasons, looking at the same types of fields.

Figure 10a shows that the April differences have moderated in southern high latitudes but increased in northern high latitudes. Figure 10b again shows values of statistical significance nearly everywhere outside the tropics. Also, the significant areas within the three convective centers have shrunken slightly. July's difference field, Figure 11a, shows a considerable decrease from April over northern high latitudes in general and over northwestern N. America in particular. In addition, tropical areas of model overestimation have migrated to the northwest somewhat following the ITCZ. The t-values for July (Figure 11b) also show a drift to the northwest of statistically significant tropical convective areas. Note that the area over central S. America is no longer significant.

October's Figures 12a and 12b show similar patterns with a slight intensification of tropical areas of overestimation and once again three tropical areas of statistical significance.

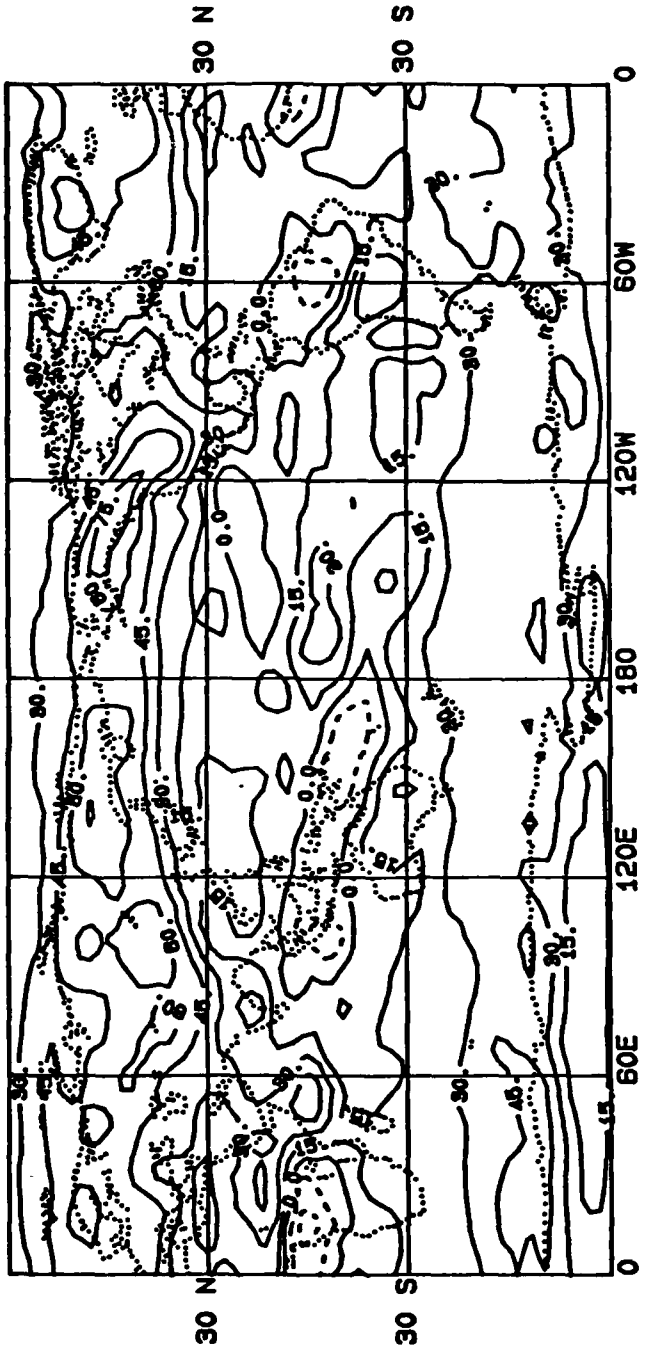

Figure 10a. April OLR difference (observed - simulated).

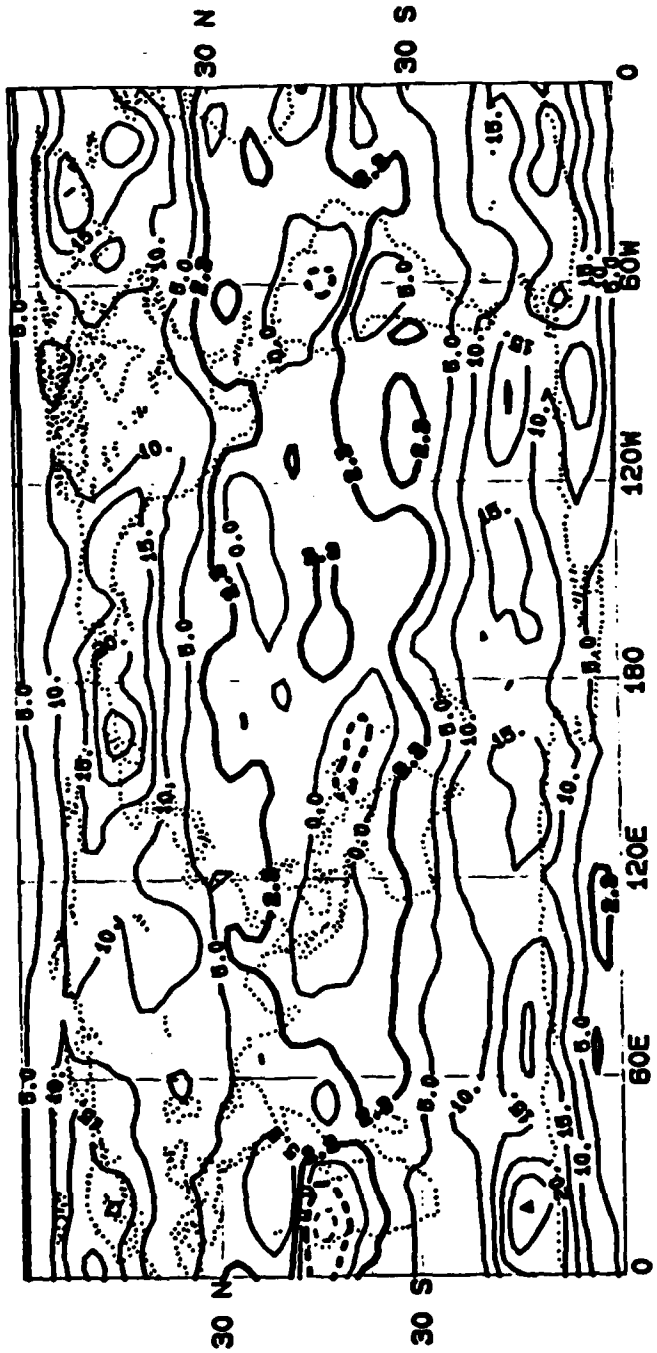

Figure 10b. April t-values.

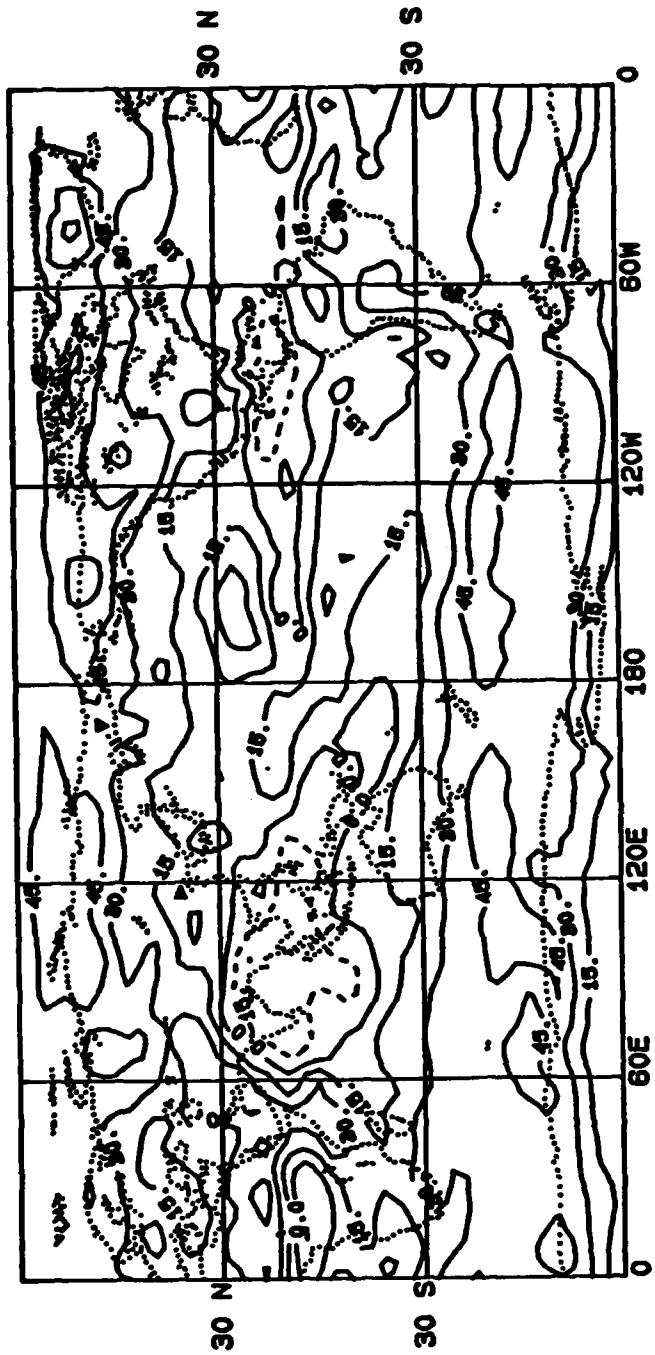

Figure 11a. July OLR difference (observed - simulated).

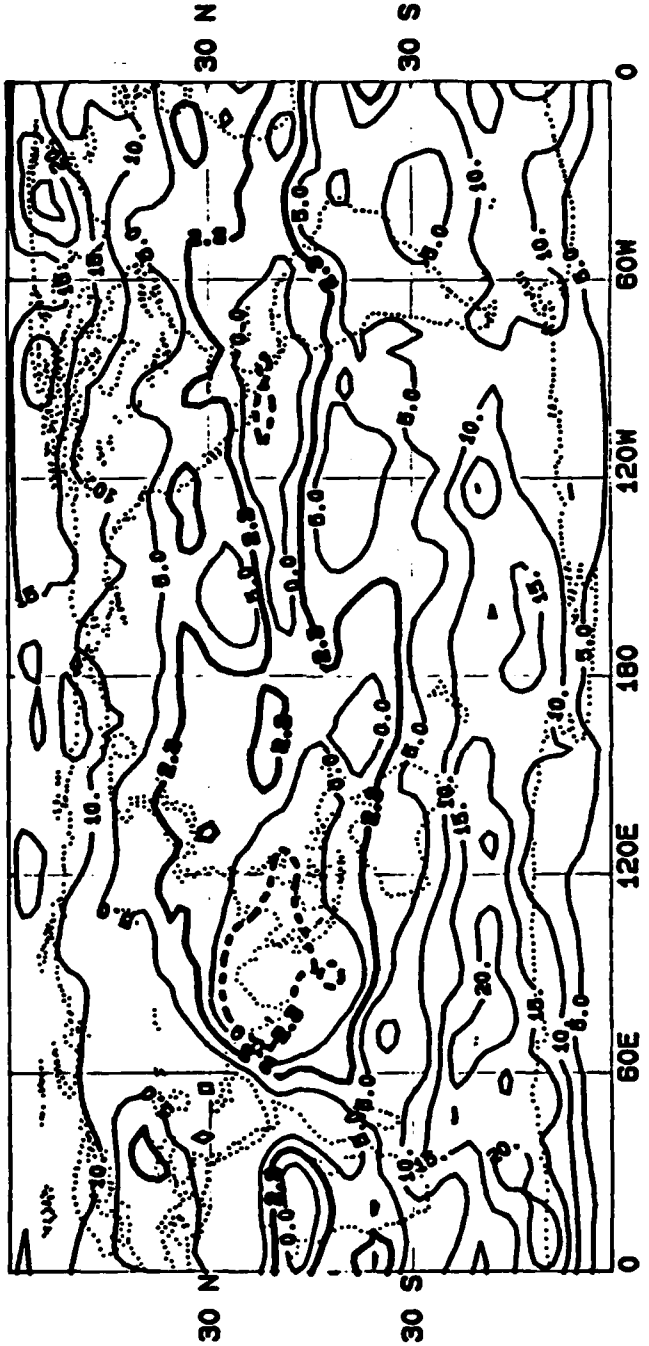

Figure 11b. July t-values.

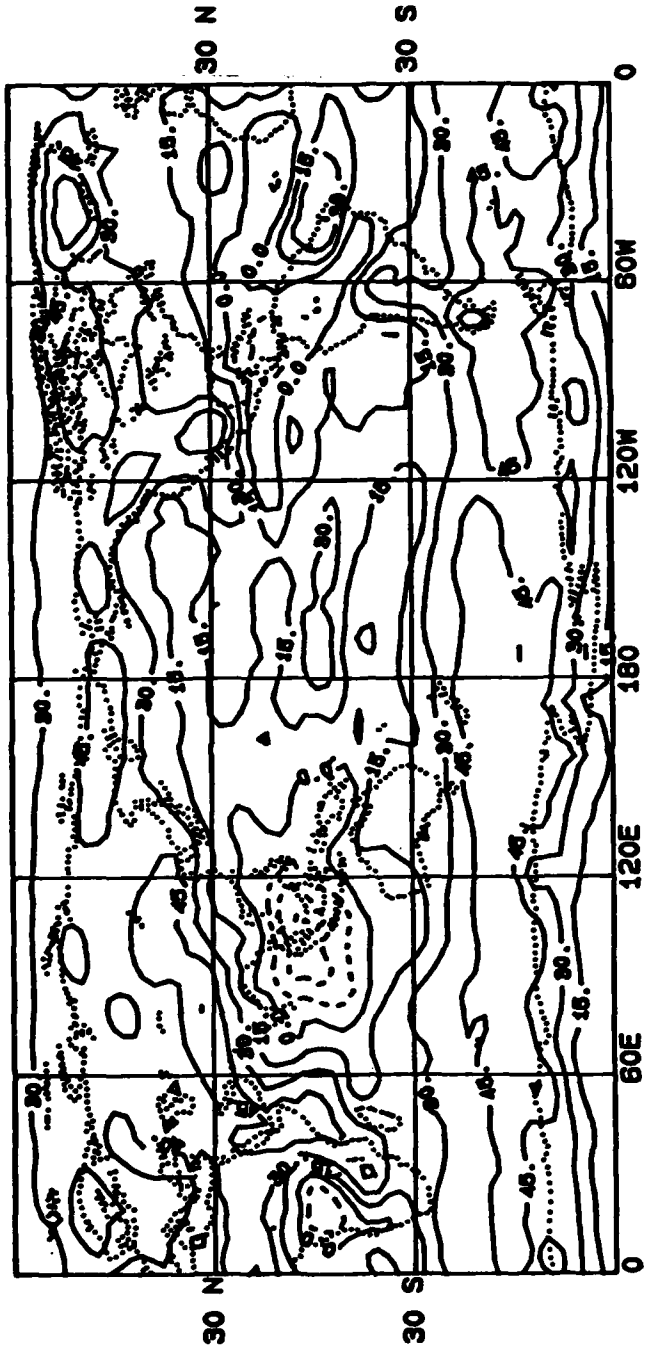

Figure 12a. October OLR difference (observed - simulated).

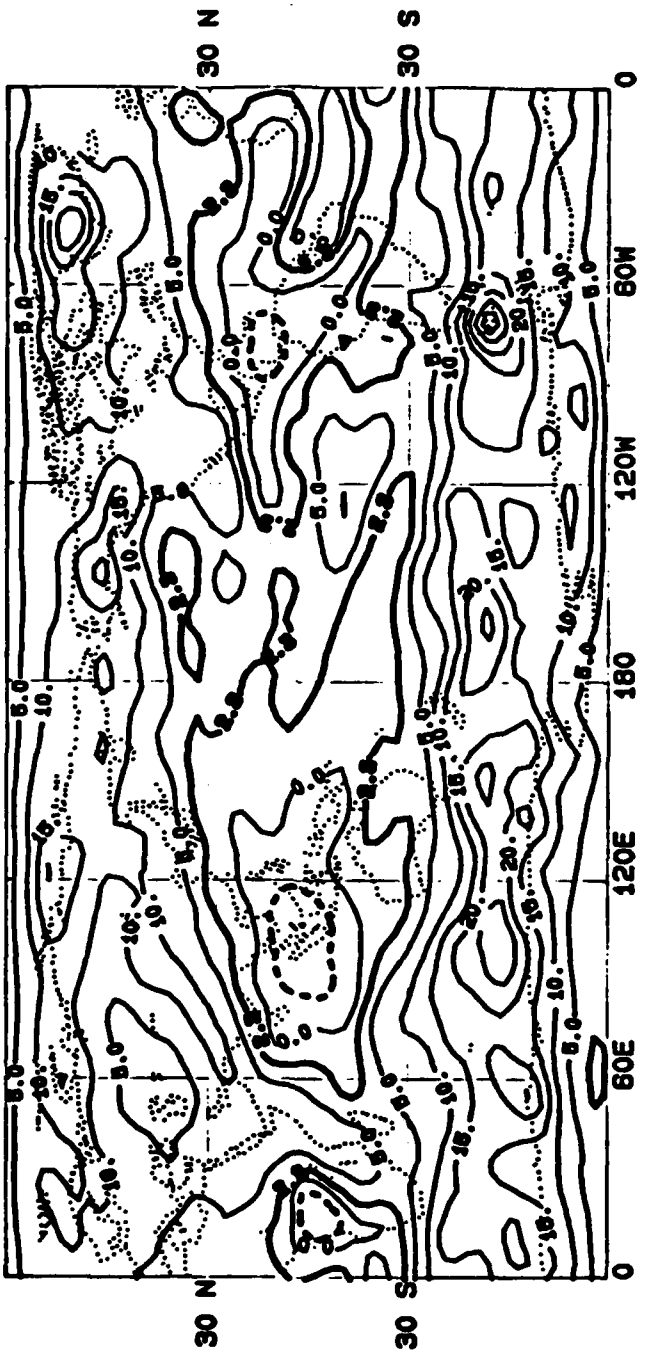

Figure 12b. October t-values.

6. CONCLUSIONS

We validated the GLAS GCM's OLR using observations with high accuracy and global density. We used conventional comparisons as well as spherical harmonic analysis and statistical procedures for validation. This provided a measure of quantitative, in addition to merely qualitative, assessments of the model's strengths and weaknesses in simulating mean outgoing longwave radiation.

The model produces low estimates of OLR at all latitudes outside the tropics. This deficiency was previously reported by Shukla, et al. (1981). The basic problem seems to lie in excessive model cloudiness as evidenced by a simulated planetary albedo of 0.40 (Randall, 1982a) compared with the observed albedo of about 0.30. However, we can now state with more confidence the degree to which the model is deficient in some areas. Global average OLR is too low by 20-23 Wm^{-2}. This represents approximately 10% of the observed global average OLR. Regional estimates fall within a range from 75 Wm^{-2} lower than observed to 45 Wm^{-2} higher than observed. High-latitude estimates in both hemispheres are consistently low while OLR in the tropical convective centers is routinely overestimated.

The dominant spherical harmonic component, (2,0), which represents the equator-pole gradient in a global average

sense, shows us that the OLR gradient is consistently too steep by about 12 Wm^{-2}. The component which represents a more seasonal than annual picture, (1,0), shows strong evidence that the model successfully simulates the observed inter-hemispheric seasonal cycle of OLR.

The model performs reasonably well in reproducing the phases and amplitudes of the component waves, particularly the zonally symmetric components. Perhaps the lower values of the zonally asymmetric component correlations and simulated amplitudes will provide some guidance as to how best to improve the model dynamics so that east-west variability can be better simulated.

Statistically, the model fares rather poorly over most of the globe with the exception of portions of the tropics, where observations show variability of OLR to be highest. The various figures presented also show how very poorly the model performs, in a statistical sense, at high latitudes.

The excessive tropical values of OLR generated by the model are surely due to radiative neglect of convective clouds. Perhaps further research along the lines of this study would provide justification for re-introducing code into the model to allow convective cloud-radiation interaction, at least in portions of the tropics.

Future research could also validate the year-to-year variability of the standard deviation of OLR. This, of course, would require a much larger sample of simulated data than was used in this study. Other possible research areas

include validation of temperatures, winds, stream functions, etc. We feel strongly that further research efforts should emphasize objective and qualitative validation procedures similar to those employed in this study.

APPENDIX I : CALCULATIONS

I. Global Standard Deviation (S_G)

$$S_G = \left[\sum_{j=1}^{N} (4\pi/360)\, s^2(j) \cos\theta_j \right]^{1/2}$$

Where,

N = number of grid points between North and South poles.

$\theta_j = [\, 90 - 4(j-1) \,](2\pi/360)$: Latitude converted from degrees to radians.

$$s^2(j) = (1/M) \sum_{i=1}^{M} [\, F(i,j) - AVG \,]^2$$

M = number of grid points along a latitude circle.

$$AVG = \sum_{j=1}^{N} (4\pi/360)\, XBAR(j) \cos\theta_j$$: Global average OLR.

$$XBAR(j) = (1/M) \sum_{i=1}^{M} F(i,j)$$: Average around latitude circle.

And F(i,j) is our field as a function of i,j grid points.

II. Monthly Standard Deviation Field (S(i,j))

$$S(i,j) = \left[(1/Y) \sum_{n=1}^{Y} (F(i,j)_n - AVGOLR(i,j))^2 \right]^{1/2}$$

Where,

Y = number years of data

$$AVGOLR(i,j) = (1/Y) \sum_{n=1}^{Y} F(i,j)_n$$

APPENDIX I : CALCULATIONS

III. % Explained Variance (EV)

$$EV = 100(AMP_{n,m})^2/S_a^2$$

IV. Correlation Coefficients

A. Total Coefficients (R(x,y))

$$R(x,y) = \sum_{n=0}^{N} [\, A_n a_n + 2 \sum_{m=1}^{m=n} (A_{n,m} a_{n,m} + B_{n,m} b_{n,m}) \,] / (s(x) s(y))$$

Where,

x and y represent the observed and simulated fields, respectively.

For our purposes, N is truncated at 15.

$$s(x) = [\, \sum_{n=0}^{N} (A_n^2 + 2 \sum_{m=1}^{m=n} (A_{n,m}^2 + B_{n,m}^2)) \,]^{1/2}$$

$$s(y) = [\, \sum_{n=0}^{N} (a_n^2 + 2 \sum_{m=1}^{m=n} (a_{n,m}^2 + b_{n,m}^2)) \,]^{1/2}$$

B. Symmetric Coefficients (Rs(x,y))

$$Rs(x,y) = \sum_{n=0}^{N} A_n a_n / [ss(x)\ ss(y)]$$

Where,

$$ss(x) = [\, \sum_{n=0}^{N} A_n^2 \,]^{1/2}$$

$$ss(y) = [\, \sum_{n=0}^{N} a_n^2 \,]^{1/2}$$

APPENDIX I : CALCULATIONS

C. Asymmetric Coefficients ($R_A(x,y)$)

$$R_A(x,y) = 2 \sum_{n=1}^{N} \sum_{m=1}^{n} (A_{n,m}a_{n,m} + B_{n,m}b_{n,m}) \; / \; [s_A(x)s_A(y)]$$

Where,

$$s_A(x) = [\, 2 \sum_{n=1}^{N} \sum_{m=1}^{n} (A_{n,m}^2 + B_{n,m}^2) \,]^{1/2}$$

$$s_A(y) = [\, 2 \sum_{n=1}^{N} \sum_{m=1}^{n} (a_{n,m}^2 + b_{n,m}^2) \,]^{1/2}$$

V. 't'-Values (t)

$$t = K \; (XBAR - YBAR)/(n_x s_x^2 + n_y s_y^2)^{1/2}$$

Where,

$$K = [\, n_x n_y (n_x + n_y - 2)/(n_x + n_y) \,]$$

and,

XBAR and YBAR represent averages of n_x and n_y years of OLR.

n_x and n_y are the number of years of observed and simulated input.

$$s_x = [\, (1/n_x) \sum_{i=1}^{n_x} (x_i - XBAR)^2 \,]^{1/2}$$

$$s_y = [\, (1/n_y) \sum_{i=1}^{n_y} (y_i - YBAR)^2 \,]^{1/2}$$

APPENDIX II : AMPLITUDES

Observed Data, January

M N	0	1	2	3	4	5	6	7	8	9	10	11	12	13	14
1	7.60	2.39													
2	25.67	1.03	2.14												
3	1.68	0.57	2.24	0.65											
4	4.12	0.92	2.37	1.94	2.13										
5	5.76	1.63	1.11	0.79	1.26	1.60									
6	5.26	1.93	2.45	2.70	0.74	0.63	0.63								
7	4.52	1.38	0.31	0.94	1.90	0.78	0.42	0.53							
8	4.44	1.00	0.81	1.79	0.47	0.72	0.41	0.02	0.72						
9	3.16	1.51	0.52	0.45	1.44	0.58	0.80	0.63	0.35	0.47					
10	1.03	2.01	1.15	0.62	1.23	0.46	0.28	0.39	0.59	0.57	0.22				
11	0.14	0.71	0.30	0.80	0.50	0.41	0.26	0.25	0.50	0.22	0.25	0.43			
12	0.09	0.39	0.44	0.90	0.59	0.14	0.53	0.11	0.36	0.30	0.18	0.19	0.34		
13	0.70	0.59	0.36	0.23	0.38	0.28	0.44	0.42	0.19	0.24	0.15	0.04	0.19	0.20	
14	0.11	0.42	0.46	0.19	0.58	0.21	0.33	0.10	0.30	0.34	0.17	0.20	0.11	0.15	0.33
15	0.15	0.31	0.24	0.57	0.13	0.14	0.25	0.46	0.33	0.19	0.13	0.19	0.44	0.29	0.16

Observed Data, April

M N	0	1	2	3	4	5	6	7	8	9	10	11	12	13	14
1	1.73	1.65													
2	25.50	1.80	1.88												
3	2.51	0.63	1.04	0.48											
4	7.10	0.90	0.70	0.92	1.85										
5	3.83	1.37	0.42	0.77	0.21	2.32									
6	3.13	2.33	1.11	1.96	0.69	0.48	0.43								
7	0.64	1.04	0.79	1.25	0.65	1.14	0.59	0.78							
8	7.52	0.60	0.54	0.92	0.87	0.81	0.31	0.08	0.57						
9	0.93	1.63	0.97	0.96	0.43	1.10	0.53	0.48	0.57	0.20					
10	3.29	1.69	1.04	0.16	0.61	0.33	0.36	0.11	0.41	0.38	0.32				
11	1.13	0.37	0.96	0.35	0.44	0.41	0.25	0.52	0.12	0.25	0.23	0.17			
12	1.54	0.83	0.71	0.58	0.21	0.31	0.32	0.23	0.32	0.32	0.46	0.21	0.33		
13	1.38	0.69	0.28	0.60	0.83	0.29	0.10	0.11	0.14	0.08	0.20	0.04	0.28	0.16	
14	0.77	0.22	0.66	0.38	0.41	0.17	0.14	0.15	0.31	0.43	0.14	0.08	0.20	0.12	0.15
15	0.05	0.37	0.35	0.61	0.59	0.18	0.22	0.19	0.28	0.22	0.12	0.16	0.22	0.15	0.02

APPENDIX II : AMPLITUDES

Observed Data, July

M N	0	1	2	3	4	5	6	7	8	9	10	11	12	13	14
1	13.40	3.00													
2	20.69	2.99	3.60												
3	7.07	1.74	2.38	0.17											
4	7.86	2.70	1.22	1.16	2.48										
5	2.37	2.78	2.43	1.77	1.24	1.66									
6	2.50	1.25	1.12	1.47	0.63	0.40	1.22								
7	6.41	0.57	0.86	1.14	0.64	0.23	1.01	0.91							
8	4.26	0.49	1.21	0.82	0.76	0.55	0.40	0.61	0.43						
9	3.18	0.74	0.80	0.79	0.60	0.24	0.73	0.35	0.58	0.28					
10	0.21	0.98	0.85	0.95	0.28	0.32	0.27	0.19	0.60	0.19	0.35				
11	1.57	0.88	1.19	0.36	1.02	0.38	0.43	0.23	0.27	0.15	0.24	0.49			
12	0.41	0.74	0.46	0.40	0.63	0.24	0.08	0.19	0.34	0.28	0.26	0.34	0.18		
13	1.67	0.71	0.11	0.72	0.69	0.39	0.25	0.17	0.11	0.24	0.26	0.07	0.41	0.32	
14	0.27	0.46	0.56	0.70	0.34	0.13	0.09	0.34	0.35	0.26	0.11	0.17	0.26	0.23	0.06
15	0.75	0.36	0.23	0.36	0.67	0.17	0.22	0.06	0.19	0.32	0.20	0.22	0.20	0.11	0.29

Observed Data, October

M N	0	1	2	3	4	5	6	7	8	9	10	11	12	13	14
1	5.05	1.17													
2	25.68	2.08	3.08												
3	2.48	0.25	2.15	0.52											
4	7.70	1.29	0.90	0.97	2.39										
5	0.61	2.31	0.73	1.28	0.44	2.14									
6	4.01	1.15	0.98	1.57	1.01	0.40	0.96								
7	4.02	1.42	0.21	1.28	0.63	0.91	0.62	0.61							
8	4.70	0.57	0.31	1.25	0.70	1.07	0.29	0.34	0.97						
9	2.20	1.92	0.63	1.01	0.65	0.82	0.39	0.58	0.16	0.71					
10	0.75	1.36	0.49	0.51	0.73	0.62	0.16	0.49	0.99	0.38	0.44				
11	1.93	1.08	0.90	0.53	0.24	0.52	0.26	0.39	0.16	0.25	0.34	0.24			
12	0.37	0.37	0.13	0.67	0.44	0.34	0.36	0.40	0.61	0.52	0.21	0.14	0.34		
13	1.68	1.01	0.26	0.37	0.19	0.58	0.25	0.33	0.20	0.23	0.30	0.18	0.16	0.06	
14	1.05	0.28	0.30	0.49	0.47	0.23	0.46	0.16	0.40	0.45	0.15	0.18	0.22	0.19	0.18
15	0.17	0.23	0.33	0.39	0.61	0.27	0.16	0.15	0.19	0.33	0.26	0.16	0.33	0.02	0.26

APPENDIX II : AMPLITUDES

Simulated Data, January

M N	0	1	2	3	4	5	6	7	8	9	10	11	12	13	14
1	6.56	0.94													
2	38.28	1.72	2.01												
3	2.34	1.59	2.93	0.93											
4	0.57	0.92	1.84	2.44	0.93										
5	3.65	1.25	0.76	1.97	1.23	0.98									
6	6.92	0.72	0.94	1.15	0.98	0.32	0.56								
7	2.07	0.74	0.95	0.89	0.67	0.07	0.06	0.60							
8	3.61	0.59	0.61	0.30	0.58	1.01	0.44	1.09	0.39						
9	1.15	1.43	0.98	0.50	0.60	0.74	0.38	0.41	0.87	0.36					
10	2.21	0.89	0.13	0.45	0.82	0.09	0.19	0.36	0.40	0.72	0.39				
11	0.02	1.34	0.21	1.17	0.68	0.32	0.20	0.49	0.23	0.36	0.62	0.38			
12	1.24	0.39	0.24	0.55	0.14	0.13	0.29	0.60	0.21	0.41	0.36	0.21	0.31		
13	0.78	0.74	0.56	0.15	0.05	0.43	0.45	0.09	0.17	0.47	0.40	0.45	0.43	0.28	
14	1.24	0.14	0.65	0.40	0.28	0.19	0.46	0.47	0.29	0.31	0.13	0.49	0.36	0.01	0.42
15	0.20	0.28	0.27	0.09	0.35	0.12	0.45	0.30	0.39	0.28	0.17	0.27	0.32	0.11	0.10

Simulated Data, April

M N	0	1	2	3	4	5	6	7	8	9	10	11	12	13	14
1	1.63	1.46													
2	38.94	2.17	1.10												
3	1.39	1.79	1.54	1.07											
4	3.45	2.01	1.08	1.17	1.26										
5	4.77	0.60	0.46	1.46	0.62	1.17									
6	6.83	0.82	0.91	1.21	0.68	0.97	0.13								
7	0.43	0.68	1.43	0.32	0.42	0.27	0.46	1.21							
8	5.52	0.22	0.70	0.89	0.18	0.58	0.39	0.96	0.39						
9	0.35	1.12	0.83	0.59	0.66	0.74	0.26	0.74	0.20	0.34					
10	2.54	1.22	0.53	0.73	1.02	0.62	0.08	0.15	0.31	0.69	0.57				
11	0.91	1.54	0.22	0.86	0.53	0.05	0.40	0.05	0.05	0.24	0.28	0.33			
12	0.39	0.57	0.38	0.26	0.29	0.53	0.33	0.58	0.20	0.40	0.38	0.24	0.20		
13	0.75	0.52	0.29	0.34	0.16	0.49	0.23	0.28	0.12	0.39	0.28	0.20	0.38	0.09	
14	0.89	0.39	0.97	0.58	0.37	0.53	0.27	0.41	0.43	0.19	0.10	0.35	0.19	0.21	0.42
15	0.54	0.39	0.46	0.42	0.31	0.42	0.37	0.35	0.20	0.24	0.11	0.20	0.29	0.03	0.08

APPENDIX II : AMPLITUDES

Simulated Data, July

M N	0	1	2	3	4	5	6	7	8	9	10	11	12	13	14
1	16.18	1.55													
2	32.67	2.55	1.00												
3	3.08	0.88	0.89	1.49											
4	5.96	3.52	0.94	0.31	0.44										
5	4.66	1.81	0.69	1.79	1.50	0.81									
6	3.78	0.44	1.36	1.50	0.68	0.33	0.47								
7	4.70	0.45	0.85	0.83	0.39	0.44	0.78	0.54							
8	3.18	0.61	0.79	0.49	0.32	0.40	0.36	0.45	0.16						
9	0.99	0.96	1.06	0.97	0.25	0.02	0.39	0.49	0.31	0.23					
10	1.22	0.58	0.92	0.99	0.32	0.47	0.40	0.34	0.43	0.20	0.39				
11	0.14	0.51	0.90	1.00	0.17	0.35	0.38	0.27	0.12	0.33	0.22	0.31			
12	0.23	0.20	0.53	0.45	0.50	0.25	0.21	0.48	0.37	0.34	0.19	0.14	0.22		
13	0.05	0.42	0.75	0.91	0.57	0.36	0.05	0.29	0.12	0.37	0.27	0.32	0.23	0.28	
14	1.26	0.43	0.54	0.44	0.36	0.19	0.23	0.35	0.10	0.29	0.24	0.08	0.04	0.21	0.16
15	0.38	0.34	0.67	0.40	0.36	0.50	0.21	0.17	0.04	0.24	0.17	0.10	0.39	0.14	0.24

Simulated Data, October

M N	0	1	2	3	4	5	6	7	8	9	10	11	12	13	14
1	6.70	0.85													
2	38.32	1.99	0.76												
3	2.30	1.27	1.71	2.33											
4	4.17	1.97	2.32	1.61	0.87										
5	1.60	0.36	1.03	1.70	0.68	1.34									
6	6.85	1.16	1.51	0.93	1.19	0.46	0.22								
7	2.20	0.68	1.18	1.48	0.26	0.13	0.16	0.66							
8	3.93	0.83	0.26	0.58	0.46	0.98	0.41	0.44	0.33						
9	0.08	0.98	0.69	0.48	0.42	0.28	0.50	0.68	0.67	0.16					
10	1.66	0.40	0.58	0.56	0.68	0.16	0.24	0.31	0.07	0.43	0.66				
11	1.29	0.68	0.61	0.64	0.04	0.05	0.41	0.17	0.36	0.39	0.53	0.35			
12	0.32	0.23	0.40	0.36	0.69	0.34	0.35	0.36	0.49	0.03	0.23	0.22	0.13		
13	1.43	0.07	0.36	0.58	0.11	0.26	0.36	0.40	0.07	0.43	0.29	0.31	0.38	0.15	
14	0.54	0.25	0.30	0.72	0.17	0.26	0.08	0.39	0.09	0.27	0.26	0.35	0.25	0.11	0.38
15	0.23	0.14	0.17	0.41	0.21	0.32	0.25	0.21	0.27	0.12	0.01	0.42	0.14	0.08	0.52

APPENDIX III : VARIANCES

Observed Data, January

N	% VARIANCE EXPLAINED	SYMMETRIC COMPONENT	ASYMMETRIC COMPONENT	CUMULATIVE VARIANCE
1	6.47	5.41	1.07	6.47
2	62.79	61.73	1.06	69.26
3	1.35	0.27	1.08	70.61
4	4.36	1.59	2.77	74.97
5	4.73	3.11	1.62	79.70
6	6.03	2.59	3.44	85.73
7	3.33	1.91	1.42	89.06
8	3.03	1.85	1.18	92.09
9	2.17	0.94	1.23	94.25
10	1.68	0.10	1.58	95.93
11	0.44	0.00	0.43	96.37
12	0.41	0.00	0.41	96.78
13	0.29	0.05	0.25	97.07
14	0.25	0.00	0.25	97.33
15	0.24	0.00	0.24	97.57
TOTALS	97.57	79.53	18.04	

Observed Data, April

N	% VARIANCE EXPLAINED	SYMMETRIC COMPONENT	ASYMMETRIC COMPONENT	CUMULATIVE VARIANCE
1	0.87	0.31	0.56	0.87
2	68.49	67.08	1.40	69.36
3	1.00	0.65	0.35	70.36
4	6.35	5.20	1.15	76.71
5	3.18	1.51	1.67	79.89
6	3.37	1.01	2.36	83.26
7	1.27	0.04	1.23	84.53
8	6.53	5.84	0.69	91.06
9	1.48	0.09	1.40	92.54
10	2.15	1.12	1.03	94.70
11	0.55	0.13	0.42	95.25
12	0.74	0.25	0.49	95.98
13	0.58	0.20	0.38	96.57
14	0.32	0.06	0.26	96.88
15	0.28	0.00	0.28	97.16
TOTALS	97.16	83.49	13.67	

APPENDIX III : VARIANCES

Observed Data, July

N	% VARIANCE EXPLAINED	SYMMETRIC COMPONENT	ASYMMETRIC COMPONENT	CUMULATIVE VARIANCE
1	18.62	16.93	1.69	18.62
2	44.46	40.33	4.13	63.08
3	6.35	4.71	1.64	69.42
4	8.89	5.82	3.06	78.31
5	4.50	0.53	3.97	82.81
6	1.92	0.59	1.33	84.73
7	4.76	3.88	0.88	89.48
8	2.46	1.71	0.75	91.95
9	1.57	0.95	0.62	93.52
10	0.64	0.00	0.64	94.16
11	1.01	0.23	0.78	95.18
12	0.36	0.02	0.34	95.54
13	0.67	0.26	0.41	96.21
14	0.31	0.01	0.31	96.52
15	0.28	0.05	0.23	96.80
TOTALS	96.80	76.03	20.77	

Observed Data, October

N	% VARIANCE EXPLAINED	SYMMETRIC COMPONENT	ASYMMETRIC COMPONENT	CUMULATIVE VARIANCE
1	2.80	2.52	0.27	2.80
2	68.01	65.27	2.73	70.80
3	1.58	0.61	0.98	72.39
4	7.67	5.86	1.81	80.06
5	2.47	0.04	2.43	82.52
6	2.95	1.59	1.36	85.48
7	2.72	1.60	1.12	88.20
8	3.13	2.19	0.94	91.33
9	1.91	0.48	1.43	93.24
10	1.02	0.06	0.96	94.26
11	0.97	0.37	0.61	95.23
12	0.42	0.01	0.40	95.65
13	0.68	0.28	0.40	96.33
14	0.40	0.11	0.29	96.72
15	0.25	0.00	0.25	96.97
TOTALS	96.97	80.99	15.98	

APPENDIX III : VARIANCES

Simulated Data, January

N	% VARIANCE EXPLAINED	SYMMETRIC COMPONENT	ASYMMETRIC COMPONENT	CUMULATIVE VARIANCE
1	2.50	2.40	0.10	2.50
2	82.65	81.87	0.78	85.16
3	1.64	0.31	1.33	86.80
4	1.26	0.02	1.24	88.05
5	1.70	0.74	0.95	89.75
6	3.13	2.67	0.46	92.88
7	0.58	0.24	0.34	93.46
8	1.14	0.73	0.41	94.60
9	0.67	0.07	0.60	95.28
10	0.57	0.27	0.30	95.85
11	0.53	0.00	0.53	96.38
12	0.25	0.09	0.16	96.63
13	0.28	0.03	0.24	96.91
14	0.30	0.09	0.21	97.20
15	0.12	0.00	0.12	97.32
TOTALS	97.32	89.54	7.78	

Simulated Data, April

N	% VARIANCE EXPLAINED	SYMMETRIC COMPONENT	ASYMMETRIC COMPONENT	CUMULATIVE VARIANCE
1	0.39	0.15	0.24	0.39
2	84.63	83.97	0.66	85.01
3	0.85	0.11	0.74	85.86
4	1.56	0.66	0.90	87.42
5	1.75	1.26	0.49	89.17
6	3.07	2.58	0.49	92.24
7	0.51	0.01	0.50	92.76
8	2.01	1.69	0.33	94.77
9	0.45	0.01	0.45	95.93
10	0.87	0.36	0.51	96.10
11	0.47	0.05	0.43	96.57
12	0.21	0.01	0.20	96.78
13	0.18	0.03	0.15	96.96
14	0.34	0.04	0.30	97.30
15	0.16	0.02	0.15	97.46
TOTALS	97.46	90.94	6.52	

APPENDIX III : VARIANCES

Simulated Data, July

N	% VARIANCE EXPLAINED	SYMMETRIC COMPONENT	ASYMMETRIC COMPONENT	CUMULATIVE VARIANCE
1	16.43	16.14	0.30	16.43
2	66.71	65.79	0.92	83.14
3	1.06	0.59	0.47	84.20
4	3.86	2.19	1.67	88.06
5	2.55	1.34	1.22	90.62
6	1.51	0.88	0.63	92.13
7	1.71	1.36	0.35	93.84
8	0.85	0.63	0.23	94.69
9	0.50	0.06	0.44	95.19
10	0.48	0.09	0.39	95.67
11	0.34	0.00	0.33	96.01
12	0.18	0.00	0.18	96.19
13	0.32	0.00	0.31	96.51
14	0.25	0.10	0.15	96.76
15	0.19	0.01	0.18	96.95
TOTALS	96.95	89.17	7.78	

Simulated Data, October

N	% VARIANCE EXPLAINED	SYMMETRIC COMPONENT	ASYMMETRIC COMPONENT	CUMULATIVE VARIANCE
1	2.60	2.52	0.08	2.60
2	83.08	82.57	0.51	85.68
3	1.42	0.30	1.12	87.10
4	2.39	0.98	1.42	89.50
5	0.86	0.14	0.71	90.35
6	3.33	2.64	0.70	93.68
7	0.79	0.27	0.52	94.47
8	1.18	0.87	0.31	95.65
9	0.35	0.00	0.35	96.00
10	0.39	0.15	0.23	96.38
11	0.33	0.09	0.24	96.72
12	0.18	0.01	0.18	96.90
13	0.27	0.11	0.16	97.17
14	0.18	0.02	0.16	97.35
15	0.12	0.00	0.12	97.47
TOTALS	97.47	90.68	6.79	

Bibliography

Abel, P., and A. Gruber,1979: An Improved Model for the Calculation of Longwave Flux at 11μm. *NOAA Tech. Rept. NESS 106*, 24 pp.

Arakawa, A., 1972: Design of the UCLA General Circulation Model. *Numerical Simulation of Weather and Climate*, Technical Report No. 7, Dept. of Meteorology, UCLA.

Arakawa, A., and V.R. Lamb, 1977: Computational Design of the Basic Dynamical Processes of the UCLA General Circulation Model. *Methods in Computational Physics*, 17, Academic Press, New York, 173-265.

Arakawa, A., M.J. Suarez, 1983: Vertical Differencing of the Primitive Equations in Sigma Coordinates. *Mon. Wea. Rev.*, 111, 34-45.

Blackmon, M.L., 1976: A Climatological Spectral Study of the 500 mb Geopotential Height of the Northern Hemisphere. *J. Atmos. Sci.*, 33, 1607-1623.

Byerly, W.E., 1893: An Elementary Treatise on Fourier's Series and Spherical, Cylindrical, and Ellipsoidal Harmonics, with Applications to Problems in Mathematical Physics. Dover Publications, Inc., New York, 287 pp.

Christidis, Z.D. and J. Spar, 1981: Spherical Harmonic Analysis of a Model-Generated Climatology. *Mon. Wea. Rev.*, 109, 215-229.

Ellingson, R.G., and R.R. Ferraro, Jr., 1983: An Examination of a Technique for Estimating Longwave Radiation Budget From Satellite Radiance Observations. *J. Clim. & Appl. Met.*, **22**, 1416-1423.

Elsasser, W. M., 1942: Harvard Met. Studies, No. 6, Harvard University Press.

Goody, R.M., 1952: A Statistical Model for Water Vapour Absorption. *Quart. J. R. Met. Soc.*, **78**, 165-169.

Goody, R.M., 1964: *Atmospheric Radiation 1: Theoretical Basis.* Clarendon Press, Oxford, 436 pp.

Gruber, A. and J.S. Winston, 1978: Earth-Atmosphere Radiative Heating Based on NOAA Scanning Radiometer Measurements: *Bull. Amer. Meteor. Soc.*, **59**, 1570-1573.

Gruber, A. and A.F. Krueger, 1984: The Status of the NOAA Outgoing Longwave Radiation Data Set. *Bull. Amer. Meteor. Soc.*, **65**, 958-962.

Janowiak, J.E., A.F. Krueger, P.A Arkin, and A. Gruber, 1985: Atlas of Outgoing Longwave Radiation Derived from NOAA Satellite Data, NOAA Atlas No. 6, U.S. Dept of Commerce, NOAA/NESDIS, Washington, D.C., 44 pp.

Krishnamurthy, V., 1982: The Documentation of the Wu-Kaplan Radiation Parameterization. *NASA Tech. Memo. 83926*, 93pp.

Moeng, C.-H, and D.A. Randall, 1982: The Radiative Impact of Cumulus Cloudiness in a General Circulation Model. Submitted to the *Mon. Wea. Rev.*.

Newell, R.E., G.F. Herman, J.M. Fullmer, W.R. Tahnk, and M. Tanaka, 1974: *Proceedings of the International Conference on Structure, Composition and General Circulation of the Upper and Lower Atmospheres and Possible Anthropogenic Perturbations*, January 14-25, 1974, Vol. 1, 17-82.

Ohring, G., A. Gruber, and R.G. Ellingson, 1984: Satellite Determination of the Relationship Between Total Longwave Radiation Flux and Infrared Window Radiance. *J. Clim. & Appl. Met.*, 23, 416-425.

Randall, D.A., Y. Sud, J. Shukla, Y. Mintz, V. Serafini, D.H. Kitzmiller, and J. Abeles, 1982: Gridded Monthly Boundary Conditions for Global Atmospheric Circulation Models. NASA Tech Memo in preparation.

Randall, D.A., 1982a: Performance of the PBL Parameterizations in the GLAS and UCLA Models. *Proceedings of the Workshop on the Planetary Boundary Layer of the European Centre for Medium Range Weather Forecasts*, Reading, England, 81-118.

Rodgers, C.D., and C.D. Walshaw, 1966: The Computation of Infra-Red Cooling Rate in Planetary Atmospheres. *Quart. J. R. Met. Soc.*, 92, 67-92.

Shukla J., D. Strauss, D. Randall, Y. Sud, and L. Marx, 1981: Winter and Summer Simulations with the GLAS Climate Model. *NASA Tech Memo 83866*, 282pp.

Somerville, R.C.J., P.H. Stone, M. Halem, J.E. Hansen, J.S. Hogan, L.M. Druyon, G. Russel, A.A. Lacis, W.J. Quirk, and J. Tenenbaum, 1974: The GISS Model of the Global Atmosphere. *J. Atmos. Sci.*, 31, 84-117.

Wark, D.Q., G. Yamomoto, and J.Lienesch, 1962: Infrared Flux and Surface Temperature Determination From TIROS Radiometer Measurements. *NSL Rpt. No. 10*, U.S. Department of Commerce, Weather Bureau.

Wu,M.-L.C., 1976: Ph.D. Thesis, Department of Geophysical Sciences, University of Chicago.